SOFC Modeling for the Simulation of Residential Cogeneration Systems

by

Michael J. Carl
B.Sc., University of Guelph, 2005

A Thesis Submitted in Partial Fulfillment of the
Requirements for the Degree of

MASTER OF APPLIED SCIENCE

in the Department of Mechanical Engineering

Supervisory Committee

SOFC Modeling for the Simulation of Residential Cogeneration Systems

by

Michael J. Carl
B.Sc., University of Guelph, 2005

Supervisory Committee

Dr. Ned Djilali, Department of Mechanical Engineering
Supervisor

Dr. Ian Beausoleil-Morrison, Department of Mechanical and Aerospace Engineering, Carleton University
Supervisor

Dr. Andrew Rowe, Department of Mechanical Engineering
Outside Member

Dr. Harry Kwok, Department of Electrical and Computer Engineering
External Examiner

Abstract

Supervisory Committee

Dr. Ned Djilali, Department of Mechanical Engineering
Supervisor

Dr. Ian Beausoleil-Morrison, Department of Mechanical and Aerospace Engineering, Carleton University
Supervisor

Dr. Andrew Rowe, Department of Mechanical Engineering
Outside Member

Dr. Harry Kwok, Department of Electrical and Computer Engineering
External Examiner

Improvements have been made to the fuel cell power module (FCPM) within the SOFC cogeneration simulation code developed under the umbrella of the International Energy Agencies Annex 42 project. The main objective of the improved model developed here is to increase generality and applicability, and to decrease reliance on empirical data. A semi-mechanistic model has been developed to represent a nominal 5 kW tubular SOFC stack power module. This model has been implemented into the building simulation software ESP-r. Results illustrating the FCPM system performance as it relates to the output power required by the building as well as results from a number of different operating scenarios are presented in this study. Actual tests performed on a 5 kW SOFC unit were used to validate the model. The simulation results are found to correlate well with experimental observations. The improved model also allows for manipulation of operational parameters such as fuel utilization, excess air ratio and temperature as well as

physical parameters such as cell dimensions and materials. Results from sensitivity and parametric simulations are also presented to demonstrate the enhanced capabilities of the model.

Table of Contents

List of Tables

List of Figures

Nomenclature

A	Constant for equilibrium constant calculation (K^{-4})
A_{cell}	*A*rea perpendicular to current flow (cm^2)
A_{int}	*A*rea perpendicular to current flow for the interconnect (cm^2)
B	Constant for equilibrium constant calculation (K^{-3})
B_o	Permeability
C	Constant for equilibrium constant calculation (K^{-2})
c	Concentration ($mol \cdot m^{-3}$)
CH_4	Chemical formula methane
C_nH_m	Chemical formula generic hydrocarbon
CO	Chemical formula carbon monoxide
CO_2	Chemical formula carbon dioxide
D	Constant for equilibrium constant calculation (K^{-1})
D_{eff}	Effective diffusion coefficient ($cm^2 \cdot s^{-1}$)
$D_{H2\text{-}H2O}$	Binary diffusion coefficient ($cm^2 \cdot s^{-1}$)
$D_{i,k}$	Knudsen diffusion coefficient ($cm^2 \cdot s^{-1}$)
Deg	Degradation term for η_{FCPM}
E	Constant for equilibrium constant calculation
E^o	Open circuit voltage (V)
E_{act}	Activation energy (kJ)
$E_{a,reform}$	Activation energy reformation rate equation ($kJ \cdot mol^{-1}$)
E_g	Energy generated within system (W)
E_h	Theoretical maximum voltage based on the LHV of the fuel (V)

E_{in}	Energy into system (W)
E_{out}	Energy out of system (W)
E_r	Nernst potential voltage (V)
E_s	Energy storage in system (W)
F	Faradays constant (coulombs $\cdot mol^{-1}$)
$\Delta f \hat{h}^{\circ}$	Standard enthalpy of formation ($J \cdot kmol^{-1}$)
g_f	Gibbs free energy (kJ)
$\dot{H}$	Enthalpy flow ($J \cdot kmol^{-1} \cdot s^{-1}$)
H_2O	Chemical formula water
H_2	Chemical formula hydrogen
h	Molar enthalpy in ($J \cdot kmol^{-1}$)
i	Current density ($A \cdot cm^{-2}$)
I_{cell}	Cell current (A)
i_L	Limiting current density ($A \cdot cm^{-2}$)
i_o	Exchange current density ($A \cdot cm^{-2}$)
J	Molar species flux ($mol \cdot cm^{-2} \cdot s^{-1}$)
K_r	Equilibrium constant gas-shift reaction
K_s	Equilibrium constant gas-shift reaction
L	Thickness (cm)
L_{cell}	Cell length (z-dir)
LHV_{fuel}	Lower heating value of the fuel ($J \cdot kmol^{-1}$)
m	Empirical coefficient (exchange current density equation)
M	Molar mass ($kg \cdot mol^{-1}$)

$M C_\rho$	Thermal capacitance ($J \cdot K^{-1}$)
n	Molar flow rate ($kmol \cdot s^{-1}$)
$\dot{N}$	Molar flow rate in ($kmol \cdot s^{-1}$)
$\dot{N}_{air}$	Molar flow rate of air to fuel cell stack ($kmol \cdot s^{-1}$)
$\dot{N}_{airstoic}$	Theoretical amount of O_2 required by the electrochemical reactions ($kmol \cdot s^{-1}$)
$n_{cells\text{-}parallel}$	Number of cells in parallel
$n_{cells\text{-}series}$	Number of cells in series
n_e	Electrons per molecule of fuel
$\dot{N}_{fuel\text{-}FCPM}$	Fuel flow rate ($kmol \cdot s^{-1}$)
$\dot{N}_{fuel\text{-}stack}$	Fuel flow rate to the stack ($kmol \cdot s^{-1}$)
$\dot{N}_{fuel\text{-}burn}$	Fuel flow rate to the stack burner ($kmol \cdot s^{-1}$)
O_2	Chemical formula oxygen
p	Partial pressure
P	Pressure (bar)
$Path_{el}$	Radial distance (circumference) of the electrolyte (cm)
P_{cell}	Cell pressure (bar)
$P_{dc,ann}$	FCPM parasitic power draw (W)
$P_{dc,comp}$	Power draw of the BOP components (W)
P_{IV}	Power loss due to voltage drop between stack and PCU (W)
P_{el}	Electrical power required by power conditioning unit (W)
P_{stack}	Electrical power produced by the fuel cell stack (W)
$q_{skinlosses}$	Heat losses (W)

R	Universal gas constant ($bar \cdot m^3 \cdot K^{-1} \cdot mol^{-1}$)
R^2	Coefficient of determination
r_{CH4}	Reformation rate methane ($mol \cdot s^{-1}$)
R_{eq}	Area specific equivalent ohmic resistance ($\Omega \cdot cm^2$)
R_{ion}	Area specific ohmic resistance ($\Omega \cdot cm^2$)
R_{ohm}	Area specific ohmic resistance ($\Omega \cdot cm^2$)
r_{por}	Pore length (cm)
T	Temperature (K)
t	Time (s)
$T_{air,in\text{-}FCPM}$	Temperature of the air entering the FCPM (K)
$T_{air,in\text{-}FCV}$	Temperature of the air entering the FCV (K)
T_{amb}	Ambient temperature (K)
T_{FCV}	Temperature of the FCV (K)
$T_{fuel,in\text{-}FCPM}$	Temperature of the fuel entering the FCPM (K)
$T_{fuel,in\text{-}FCV}$	Temperature of the fuel entering the FCV (K)
$T_{product\text{-}FCPM}$	Temperature of the product gases leaving the FCPM (K)
$(UA)_{eff}$	Heat loss coefficient for radiation and convection ($W \cdot K^{-1}$)
U_f	Fuel utilization rate
V_{act}	Activation polarization (V)
V_{cell}	Fuel cell voltage (V)
V_{conc}	Concentration polarization (V)
V_{ohm}	Ohmic losses (V)
$V_{polarization}$	Polarization voltage losses (V)

V_{SR}	Stack resistance voltage (V)
x	Molar flow rate methane (kmol·s^{-1})
y	Molar flow rate carbon monoxide (kmol·s^{-1})
z	Molar flow rate hydrogen (kmol·s^{-1})

Greek Letters

α_1	Constant reformation rate equation
α_2	Constant reformation rate equation
β	Charge transfer coefficient
β_i	Heat transfer coefficient
γ	Pre-exponential factor
γ_{reform}	Pre-exponential factor reformation rate equation (mol·s^{-1})
γ_{H2}	Ratio of Binary to total diffusion
γ_{H2O}	Ratio of Binary to total diffusion
δ	Ratio of Knudsen to total diffusion
ε	Porosity
ε_0	Calibration coefficient for η_{FCPM} calculation (W)
ε_1	Calibration coefficient for η_{FCPM} calculation (W^{-1})
ε_2	Calibration coefficient for η_{FCPM} calculation (W^{-2})
ε_{ann-0}	Calibration coefficient for BOP power draw (W)
ε_{ann-1}	Calibration coefficient for BOP power draw (W^{-1})
ε_{IV-0}	Calibration coefficient for BOP power draw (W)
ε_{IV-1}	Calibration coefficient for BOP power draw (W^{-1})

η_{FCPM}	Efficiency of the fuel cell power module
η_{FCS}	Efficiency of the fuel cell stack
η_{stack}	Stack efficiency
θ	Temperature difference (K)
λ_{air}	Excess air ratio
μ	Viscosity ($g \cdot cm^{-1} \cdot s^{-1}$)
ν	Diffusion volume (cm^3)
τ	Tortuosity
σ	Conductivity ($\Omega^{-1} \cdot cm^{-1}$)
τ_t	Time constant (s^{-1})
χ	Mole fraction

Superscripts

an	Anode
ca	Cathode
I	Inlet condition
i	Placeholder for species (i.e. H_2, CH_4 ect.)

Subscripts

A-B	Molecules participating in binary diffusion
air	Air entering the system
an	Anode
ca	Cathode

el	Electrolyte
fuel	Fuel entering the system
I	Inlet condition
i	Placeholder for species (i.e. H_2, CH_4 ect.)
int	Interconnect
products	Product gases leaving the system
stack-burn	Referring to the stack burner

Abbreviations

1D	One dimensional
2D	Two dimensional
3D	Three dimensional
BOP	Balance of plant
CAD	Computer aided design
DGM	Dusty-gas method
ECBCS	Energy Conservation in Buildings and Community Systems programme
FCPM	Fuel cell power module
FCS	Fuel cell stack
FCT	Fuel Cell Technologies
FCV	Fuel cell control volume
FM	Fick's model
HRV	Heat recovery ventilator
IEA	International Energy Agency
NRCan	Natural Resources Canada

OCV	Open circuit voltage
OPA	Ontario Power Association
PCU	Power conditioning unit
SOFC	Solid oxide fuel cell
STCR	Steam to carbon ratio

Acknowledgments

Thanks to Dr. Ned Djilali and Dr. Ian Beausoleil-Morrison, for the opportunity to work on this project and their guidance throughout.

To my parents (Leon and Cindy), my brother (Andy), Erin, the rest of my family and friends, thank you for your love and support leading up to and during the last two years.

NRCan and NSERC are also deserving of thanks, as without their generous financial contributions this work could not have taken place.

Chapter 1

Introduction

1.1 Motivation

1.1.1 The Case for Residential Cogeneration

Solid oxide fuel cells (SOFC) are currently the subject of much interest from the research community. This is because, 1) SOFCs have a high electrical energy conversion efficiency compared to other similar technologies [Singhal and Kendall, (2004)] 2) SOFCs operate at 800-1000^{o}C generating quality thermal energy, which can be used for further electrical conversion or heating 3) SOFCs can use a number of different fuels including hydrogen, methane, carbon monoxide and other hydrocarbons 4) SOFCs offer reduced emissions over other technologies because of their increased efficiency and depending on the type of fuel, lack of combustion products.

Some SOFC applications researchers have focused on include; small scale electricity generating plants (100kW), bottoming cycle electricity generating plants, and combined heat and power production (or cogeneration). Each of the above mentioned topics is a worthwhile area of research; however, cogeneration is of particular interest because it can offer the highest over all energy efficiency. This is accomplished through the high electrical conversion efficiency of the SOFC unit itself combined with the use of the

thermal energy given off by the unit for heating. As a result cogeneration offers an intriguing alternative to current power and heat generation technologies.

SOFC cogeneration is possible with any size plant, from residential (1-5kW) to power plant (100-1000kW). Residential systems offer more immediate promise because they can easily be incorporated into existing heating systems. On the other hand the power plant scale build would require the installation of a district heating system, which is both costly and difficult to do if a retrofit is necessary. Residential systems also offer the advantages of distributed power. According to the OPA distributed power can help to reduce peak demands as well as reduce transmission and distribution congestion [OPA, (2007)]. Therefore, residential cogeneration has a distinct advantage over the plant scale for becoming a viable electricity and thermal production technology.

Despite the above mentioned advantages of residential cogeneration the consumer sector has not embraced the technology. Companies have been optimistic developing prototypes and even fully commercial units. But, these units have not been able to make an impact on consumers because, of issues surrounding cost, reliability, system performance and sizing. It is hoped that as researchers improve designs, utilize more cost effective materials, and improve reliability SOFCs will break into the market.

Researchers are using both experimental and computational techniques to improve SOFCs. Experimentation can help with prototype, real world reliability and material testing. Computational analysis can offer design and material insight at a much lower

cost then experimentation. Entire system simulations can also be used to determine novel applications such as combined cycle plants [Chan et al., (2003)], system sizing, long term cost analyses and comparisons to other technologies. Both experimental and computational research is necessary to successfully demonstrate a technology; with the current research focusing on the latter.

1.1.2 Current Cogeneration model and Need for Improvements

For the purpose of evaluating the use of SOFC cogeneration systems serving residential buildings, an integrated modeling approach accounting for the performance of the coherent SOFC cogeneration device as well as its interaction with the building environment is required. The development of such a model was one of the objectives of Annex 42 of the International Energy Agency's Energy Conservation in Buildings and Community Systems programme (IEA/ECBCS). Natural Resources Canada (NRCan) is a member of Annex 42. NRCan developed a generic model to represent the SOFC cogeneration system (Annex 42 model). The Annex 42 model was then implemented in the building simulation software ESP-r [Kelly and Beausoleil-Morrison, (2007)]. ESP-r is an open source building simulation software tool available at http://www.esru.strath.ac.uk/.

The Annex 42 model consists of 12 control volumes. Each control volume represents a different system component, i.e. the air supply blower, fuel compressor, the heat recovery device, etcetera. A full description of each of the control volumes is given in [Kelly and Beausoleil-Morrison, (2007)]. The Annex 42 model allows in principle the simultaneous

evaluation of both the thermal and electrical characteristics of the system. The focus of this work is to improve the Annex 42 model, via reworking how the model characterizes the performance of the fuel cell power module (FCPM). The FCPM consists of the SOFC stack as well as balance of plant (BOP) components. The BOP components can vary between designs, Figure 1.1 presents one possible configuration.

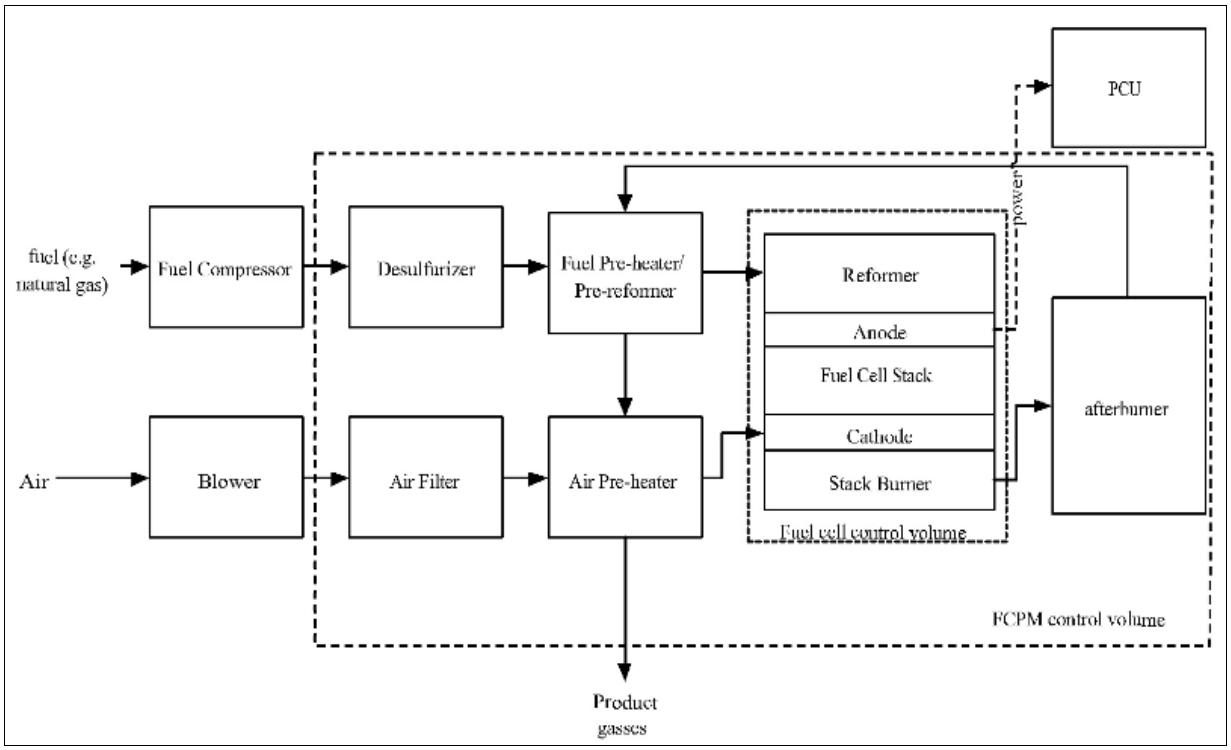

Figure 1.1 Schematic giving generic configuration for the FCPM.

Presently, in the Annex 42 model, the FCPM electrical efficiency is used to determine pertinent system characteristics such as the fuel/air supply rate and the parasitic losses of the FCPM. However, this key design component is calculated using curve fitting equation [Kelly and Beausoleil-Morrison, (2007)]:

$$\eta_{FCPM} = (\varepsilon_0 + \varepsilon_1 P_{el} + \varepsilon_2 P_{el}^2) - Deg \tag{1.1}$$

where η_{FCPM} is the FCPM electrical efficiency, ε_i are the empirical coefficients, which can be determined experimentally and *Deg* is the degradation term(discussed further in Chapter 2), P_{el} is the electrical power required by the power conditioning unit (PCU). This equation was calibrated using experimental results collected by NRCan on fuel cell technologies (FCT) 5kW SOFC system. Therefore, the Annex 42 model can only be used with certainty within the limits of those experiments; i.e. the corresponding P_{el}, access air ratio, fuel utilization and temperature ranges. In other words, only systems calibrated using experimental data can be considered; hypothetical systems can not be evaluated, limiting the model's power as a simulation tool within ESP-r.

1.2 Literature Review- SOFC Modeling Techniques

For any researcher attempting to model an SOFC the electrochemistry of the reactions, thermal, electronic and ionic properties of the materials, as well as fuel and oxidant flow must be considered. As a result, SOFC modeling is a multi-disciplinary field requiring expertise from chemists and electrical and mechanical engineers alike. Modeling of a SOFC can range from a simple thermodynamic set of equations [Akkaya, (2007), Chan et al., (2001), Yoon et al., (2007), Ivanov, (2007), Calise et al., (2006), Tanaka Kim et al., (2000), Campanari (2001)] to a system governed by species, energy, and momentum transport [Suwanwarangkul et al., (2004), Damm and Fedrov, (2006), Nikooyeh, (2007)], Bessler, (2007)]. Each method has its place in research depending on the nature of the problem and desired outputs of the model.

The following sections present an examination of SOFC modeling techniques. Hydrogen reformation is first analyzed as it pertains to SOFCs. Cell level models are then discussed in great detail. Models ranging from zero-dimensional to three-dimensional (3D) are considered. Finally, modeling as it pertains to the stack and system level is explored. The literature review focuses on tubular SOFCs as they are the subject of the current research. Figure 1.2 presents a general schematic of a tubular SOFC. In the discussion of the various models the radial coordinate system will be used. The direction running along the length of the tube will be considered the z-dir, the radius of the tube the r-dir and the curvature of the tube the θ-dir. The modeling techniques described herein will be used to develop an improved FCPM representation for use in the Annex 42 model.

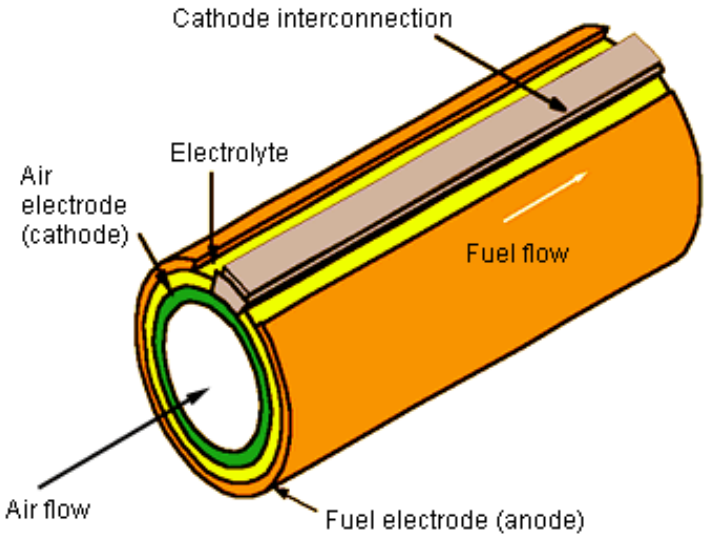

Figure 1.2 Schematic of Siemens Westinghouse tubular SOFC cell (source: http://www.powergeneration.siemens.com/products-solutions-services/products-packages/fuel-cells).

1.2.1 Fuel Reformation

SOFCs can operate using a variety of fuels; the most common being hydrogen and natural gas (methane), although carbon monoxide and most hydrocarbons can also be used. If methane or hydrocarbons are used as the fuel source then they must first be reformed to produce hydrogen and carbon monoxide. Any model which uses methane or a hydrocarbon as its fuel must consider the reformation reactions. Both indirect and direct internal reformers are used in SOFCs [Larminie and Dicks, (2003)]. A pre-reformer is also often used which increases the temperature of the gas stream as well as adding water vapour from the exhaust of the SOFC [Sanchez et al., (2008)]. The following reactions take place in the reformation process [Larminie and Dicks, (2003)]:

$$CH_4 + H_2O \rightarrow CO + 3H_2 \tag{1.2a}$$

$$C_nH_m + nH_2O \rightarrow nCO + (\frac{m}{2} + n)H_2 \tag{1.2b}$$

$$(n)CO + (n)H_2O \rightarrow (n)CO_2 + (n)H_2 \tag{1.3}$$

$$H_2 + \frac{1}{2}O_2 \rightarrow H_2O \tag{1.4}$$

Reaction 1.2a is the reformation reaction for methane. This reaction can be generalized for any hydrocarbon as given by Equation 1.2b. Reaction 1.3 is the gas-shift reaction, where a portion of the reformed CO reacts with water to produce additional hydrogen. This reaction is fast and weakly exothermic and can be evaluated using equilibrium [Nagata et al., (2003)]. Reaction 1.4 is the electrochemical reaction which takes place in the SOFC. Lisbona et al. (2007) found that the remaining CO from the gas-shift reaction does not produce electricity in the SOFC and is subsequently neglected in most electrochemical models.

The above reactions all require steam to prevent carbon from forming on the reaction sites [Sanchez et al., (2008)]. This water can be recycled from the exhaust of the SOFC or it can be supplied into the system. The amount of water used in reformation is usually expressed in terms of the ratio of water to carbon or "steam to carbon ratio" [Sanchez et al., (2008)]:

$$STCR = \frac{n_{H2O}}{n_{CH4} + n_{CO}} \tag{1.5}$$

Where STCR is the steam to carbon ratio and *n* is the molar flow rate of the gases as they enter the reformer or pre-reformer. The steam to carbon ratio can have a large influence on reformation performance as found by [Sanchez et al., (2008)]. Sanchez et al. (2008) reported that a steam to carbon ration of at least two is necessary to prevent atomic carbon from forming on the reaction sites. However steam to carbon ratios above 3.5 are also damaging as the dilution in the hydrogen content in the fuel stream will reduce cell voltage.

Although the gas shift reaction is treated under equilibrium conditions in the literature there is variance in the method for evaluating the reformation reaction [Lisbona et al. (2007)]. The three approaches used to evaluate the methane reformation reaction are: 1) to assume that the reaction is completely developed and to only consider the equilibrium of the gas shift reaction [Campanari, (2001), Lisbona et al., (2007)]: 2) to treat the reformation as well as the shift reaction with equilibrium [Chan et al., (2002), Zink et al., (2007), Massardo and Lubelli, (2000)], and 3) to use reaction kinetics for the reformation reaction [Campanari and Iora, (2004), Nagata et al., (2001), Sanchez et al., (2008)]. In

the first scenario only the gas shift reaction is considered in the model simplifying the problem. There is evidence that this approach is reasonable considering the work of Sanchez et al. (2008) which found that methane is mostly reformed at the cell entrance. Within the first tenth of the cell length less then 5% mole fraction remains and by the half way point less than 1% persists. Therefore, in situations such as zero-dimensional models where no dimensions are given to the SOFC this first simplest approach is acceptable.

For the case of equilibrium analysis, the following two equations are used to evaluate the equilibrium constants of the reformation and gas shift reactions (Equations 1.2a and 1.3):

$$K_r = \frac{p_{H_2}^3 p_{CO}}{p_{CH_4} p_{H_2O}} \tag{1.6}$$

$$K_s = \frac{p_{H_2} p_{CO_2}}{p_{CO} p_{H_2O}} \tag{1.7}$$

where p_i is the partial pressure of the respective gas and K is the equilibrium constant. The K values for both the reformation and shifting reaction have been determined by Bossel et al (1992) as a function of temperature:

$$\log K = AT^4 + BT^3 + CT^2 + DT + E \tag{1.8}$$

where T is the temperature of the reaction and A-E are constants.

Given known inlet molar flow rates for the gases and known fuel utilization for the system Chan et al. (2002) have determined a method for solving Equations 1.6 and 1.7. They used x, y, and z to represent the molar flows of methane, carbon monoxide and

hydrogen in the reactions. Re-writing Equations 1.6 and 1.7 in terms of molar flow rates and the electrochemical reaction (Equation 1.4) for determination of the hydrogen flow the following equations are developed:

$$K_r = P_{Cell}^2 \frac{(CO^I + x - y)(H_2^I + 3x + y - z)^3}{(CH_4^I - x)(H_2O^I - x - y + z)(CH_4^I + H_2O^I + 2x)^2} \tag{1.9}$$

$$K_s = \frac{(CO_2^I + y)(H_2^I + 3x + y - z)}{(CO + x - y)(H_2O^I - x - y + z)} \tag{1.10}$$

$$z = U_f(H_2^I + 3x + y) \tag{1.11}$$

where the chemical symbols represent the molar flow rates, P_{cell} is the pressure of the cell, and I stands for the inlet conditions. Equations 1.9-1.11 are a series of non-linear equations which must be solved using numerical methods such as the Newton-Raphson approach, MATLab or other computer software. It should be noted that in the literature there were many instances where Equation 1.9 was not properly written [Chan et al. (2002), Massardo and Lubelli, (2000)]. In these cases the exponent on the partial pressure of hydrogen was not carried through (one instead of three used). It is possible that a typo was made in one paper which was then copied over. Nevertheless, caution should be used when considering the results of these papers.

Finally [Sanchez et al (2008), Nagata et al., (2001)] utilize reaction kinetics to describe the rate of conversion of methane, and then equilibrium for the shift reaction. The general form of the methane reaction rate equation is given by

$$r_{CH4} = \gamma_{reform} p_{CH_4}{}^{\alpha 1} p_{H_2O}{}^{\alpha 2} \exp(\frac{-E_{a,reform}}{RT}) \quad (1.12)$$

where γ is the pre-exponential factor, $E_{a,reform}$ is the activation energy in and α_1 and α_2 are constants. The dependence of Equation 1.12 on empirically determined coefficients has lead to varying results in the literature. Sanchez et al. (2008) compared the coefficients from two methods [Achenbach, (1994), Ahmed and Foger (2000)] of evaluating Equation 1.12 as well as equilibrium conditions and found that there was a substantial discrepancy. Sanchez et al (2008) proposed a mixture of the two methods, i.e. both kinetics and equilibrium. Based on their findings the mixed model was recommended for multi-dimensional analyses, where as equilibrium is appropriate for zero-dimensional modeling [Sanchez et al., (2008)].

1.2.2 SOFC Unit Cell Modeling

Within the literature reviewed it was found that most SOFC modeling research pertains to the unit cell level rather then stack or system. Unit cell models range in complexity from dimensionless empirical equations to three-dimensional (3D) simulations solving energy, mass, momentum and species transport from first principles. Logically as the complexity of the model increases so does the simulation time and the knowledge of the operation principles required by the user. For this reason it is important to understand the output requirements of a model before the method is chosen to prevent an overly-cumbersome representation of the system. For example if the temperature distribution is needed to examine the thermal expansion characteristics of a novel electrolyte or electrode material, then a detailed energy balance model using simulation software must be used. On the

other hand if an economic evaluation of the energy provided by an SOFC gas turbine combined cycle plant over the course of a decade is being examined then a zero-dimensional model is sufficient.

1.2.2.1 Model Complexity

In order to properly evaluate and compare different models, model dimensionality must be defined. In the case of SOFC modeling because of the complex nature of the problem the domain or dimensions can be different for separate parameters. For example, a model may have one-dimensional (1D) species diffusion, two-dimensional (2D) ohmic resistance calculations, but still be limited to a global determination of the cell voltage without resolution of the special distribution. In this case the model would be considered zero-dimensional. Zero-dimensional means that the entire SOFC cell is looked at as one volume, where reactants enter, and then leave and uniform voltage and current are produced. A 1D model would evaluate current species concentration etcetera along one direction usually the z-dir, and so on for 2D and 3D.

Generally, the dimensionality of a model is related to its capabilities and utilization. Zero-dimensional models give voltage, current, power, fuel and oxidant information with respect to the whole cell. 1D models can solve for temperature as well as voltage and current distributions along the length (z-dir) of the SOFC tube. Both 1D and zero-dimensional models can help improve stack operation and insulation as well as temperature and gas recycle management [Sanchez et al., (2008), Bove et al., (2004), Campanari and Iora, (2004), Nagata et al., (2001), Jiang et al. (2006), Jia et al. (2007)].

They can also be used at the stack and system level to evaluate cost, compare technologies, and application testing. 2D models which provide further accuracy and detail to the temperature and voltage/current distribution also give some consideration of the reacts/products behaviour at the reaction sites and species distribution throughout the cell (r-dir). These more detailed models can help optimize designs, but require CFD or finite-element analyses (FEA) software [Suwanwarangkul et al. (2005)]. Finally 3D models provide temperature, species, current and voltage information throughout the entire cell. Like 2D, 3D models require the use FEA, CFD or other numerical methods. 3D models are used mostly for detailed design of cell components. Since most system level models incorporate many component which can not all be modeled in CFD or FEA software, 2 and 3D models are not considered for the present research [Sanchez et al., (2008), Bove et al., (2004), Campanari and Iora, (2004), Nagata et al., (2001), Jiang et al. (2006), Jia et al. (2007)].

The use of zero-dimensional SOFC cell models is primarily at the system level where detailed current, voltage or temperature distribution information is not required, examples include the works of [Chan et al. (2001), Chan et al. (2002), Chan et al. (2003) , Nagata et al., (2001), Akkaya, (2007)]. 1D models can also be used in these situation, if distributions of temperature, current, voltage, or species concentration ($mol \cdot m^{-3}$) is desired along the length of the cell [Sanchez et al., (2008), Bove et al., (2004), Campanari and Iora, (2004), Nagata et al., (2001), Jiang et al. (2006), Jia et al. (2007)]. In the case of the current research, control volume analyses are used for the other system components within the Annex 42 model. These other control volumes neither give nor

require information other then absolute current, voltage, temperature ect. Furthermore, the desired output is on the order of total energy used in a day, month or year. Therefore a zero-dimensional model is appropriate for the current research.

The following section will present a review of literature focusing on the electrochemical treatment of the SOFC for a zero-dimensional model. The material is also applicable to 1D models; In the case of 1D models the electrochemical equations are solved along the z-dir rather then over the entire cell.

1.2.2.2 Electrochemical Analyses

SOFCs generate voltage due to an electrochemical reaction. The voltage is related to the current density of the cell, and degrades as current density is increased. The voltage degradation is termed polarization or loss and is also a function of current density such that:

$$V_{Cell} = E_r - V_{polarization}(i) \tag{1.13}$$

Where V_{Cell} is the voltage produced by the cell, $E_r$is the Nernst potential voltage, $V_{polarization}$ are the different polarization losses which are a function of i the current density. The losses in a SOFC can be split into three different categories; 1) activation losses which occur at both the cathode and the anode, 2) ohmic losses at the electrodes as well as through the electrolyte and interconnect, and 3) finally concentration losses or mass transport losses due to diffusion limitations in both the cathode and anode [Singhal and Kindell (2004), Larmanie and Dicks, (2002)].

Nernst Potential

The maximum voltage that a fuel cell can achieve occurs when no current is being drawn; this scenario is termed the open circuit voltage (OCV). This voltage is a function of the Gibbs free energy for the products and reactants in Equation 1.4 [Larmanie and Dicks, (2002)]:

$$E^o = \frac{-\Delta \bar{g}_f^o}{n_e F} \tag{1.14}$$

Where E^o is the OCV, g_f is the Gibbs free energy for the reaction, n_e is the number of electrons per molecule of fuel and F is faradays constant. Gibbs free energy is temperature dependant with E^o decreasing as temperature increase. Equation 1.14 does not consider the effects of concentration or the partial pressures of the reactants and products. If they are considered the E_r term in Equation 1.13 becomes:

$$E_r = E^o + \frac{RT}{n_e F} \ln\left(\frac{p_{H_2} p_{O_2}^{\frac{1}{2}}}{p_{H_2O}}\right) \tag{1.15}$$

Equation 1.15 gives the reversible or theoretical maximum voltage at a given temperature and pressure. With few exceptions (e.g [Bessler et al., (2007)] in the literature reviewed the Nernst potential is used as the maximum theoretical cell voltage.

Activation Polarization

During the electrochemical reaction of a SOFC, oxygen must undergo a charge transfer from a neutral species to an ion; similarly hydrogen must be converted from a neutral species to an ion and back to a neutral species (water). These reactions are quite complex and involve many different steps including surface adsorption, desorption and surface

diffusion [Singhal and Kindell (2004)]. The reactions occur at what is termed the triple phase boundary (TPB). The TPB is where the micro-pores of the anode or cathode meet the electrolyte and the gas [Singhal and Kindell (2004)] or the electrocatalyst-electrolyte interface [Yoon et al., (2007)]. There are numerous models to describe the different charge transfer reactions mechanisms [Singhal and Kindell (2004)]; however, an exact representation of the reaction has yet to be developed [Singhal and Kindell (2004)]. There is a voltage loss associated with charge transfer, this voltage loss is termed the activation polarization. The Butler-Volmer equation gives the state of the science representation of activation polarization:

$$i = i_O\left[\exp\left(\frac{\beta n_e F V_{act}}{RT}\right) - \exp\left(\frac{-(1-\beta)n_e F V_{act}}{RT}\right)\right] \tag{1.16}$$

where i_o is the exchange current density, β is the transfer coefficient, V_{act} is the activation voltage loss, T is the temperature and R is the universal gas constant. Typically for fuel cells the transfer coefficient is 0.5 [Nehter, (2006), Akkaya, (2007), Chan et al., (2001), Yoon et al., (2007)]. There are two approaches used in literature to evaluate the Butler-Volmer equation. 1) At low current densities the Butler-Volmer equation is approximately linear. At high current densities the Tafel equation is valid [Campanari, (2001), Chan et al. (2001), Kim et al. (1999)]. 2) If the charge transfer coefficient is 0.5, Equation 1.16 can explicitly be solved. The resulting expression is an Arcsine relation of current to exchange current density. The latter represents a more accurate method for evaluating the Butler-Volmer equation and is used in most recent literature [Yoon et al. (2007), Nehter, (2006), Chan and Ding, (2005), Chan et al., (2003)]. The exchange

current density (i_o) can be approximated using the following semi-empirical relationship [Campanari and Iora, (2004), Chan et al. (2003), Yoon et al., (2007), Akkaya, (2007)]:

$$i_{o,an} = \gamma_{an} p_{H_2} p_{H_2O}{}^{m} \exp\left(-\frac{E_{act,an}}{R\,T}\right) \tag{1.17}$$

$$i_{o,ca} = \gamma_{ca} p_{O_2}{}^{0.25} \exp\left(-\frac{E_{act,ca}}{R\,T}\right) \tag{1.18}$$

where γ_{an} and γ_{ca} are the pre-exponential coefficients m is an empirical coefficient and E_{act} is the activation energy, which is taken from literature. There is some debate as to the validity of these coefficients. Campanari and Iora (2004) found that the activation energies range in literature specifically, for the anode from 100-140 kJ/kg and 117-160kJ/kg for the cathode. Due to the exponential nature of the equations, these ranges in value can lead to significant changes in the activation polarization term. The exact effect of the activation energies will be discussed further in the sensitivity chapter (4) of this work.

Ohmic Losses

Ohmic losses are caused by the electron charge transfer in the electrodes and interconnect and ion transfer in the electrolyte [Akkaya, (2007)]. These processes are governed by ohms law. Resistively or conductivity (electronic and ionic) of the SOFC materials are used to create an equivalent resistance. Three approaches for generating equivalent resistance were found in the literature. The first is to use a constant value or fit the resistance to data [Yoon 2007, Krumdieck et al., (2004), Padulles et al., (2000)]. The second is given by the following equation:

$$V_{ohm} = i(R_{ohm,\text{int}} + R_{ohm,an} + R_{ohm,cz} + R_{ion,el}) \quad (1.19)$$

where V_{ohm} are the ohmic losses R is the area specific resistance, for the interconnect (*int*), anode (*an*), cathode (*ca*) and ionic resistance for the electrolyte (*el*). The above equation is used in the majority of zero-dimensional modeling [Chan et al. (2001), Akkaya, (2007)]. The third approach is to use an equivalent circuit to represent the SOFC. The third method provides the most accuracy for equivalent resistance as it most resembles the actually situation. An equivalent circuit analysis is utilized in the current research.

Both the additive resistance and equivalent circuit method require material conductivity. Conductivity is temperature dependent, for typical SOFC materials equations based on temperature have been developed by Ferguson et al. (1996) and the Westinghouse report, (1981). Evaluation of these equations demonstrated that the electrolyte conductivity is highly temperature dependent, and can be a significant loss term when the SOFC is too cold. Therefore, ohmic losses stress the issue of accurately representing the cell temperature.

Concentration Polarization

Concentration polarization is caused by the mass transport limitations of the reactants and products at the anode and cathode. This phenomenon can be described considering isothermal transport of gaseous species through porous electrodes [Virkar et al. (2000)]. The transport of the reactants and products to the reaction sites can be evaluated using the dusty-gas model (DGM) or Fick's law of diffusion. The DGM combines the Maxwell-Stefan model for continuum diffusion with Knudsen free-molecular transport.

Convective transport was also included during the derivation of the DGM model but was neglected because total pressure change within the pores of the electrodes was taken as zero therefore negating the convective effects on the transport [Suwanwarangkul et al., (2003)]. Suwanwarangkul et al. (2003) found that the DGM provided the more accurate results then Fick's model (FM) or the Maxwell-Stefan model alone. However, the DGM required numerical computation where as the other two methods could be solved analytically. Zero-dimensional models typically use the FM approach or a simplification of the DGM [Chan et al. (2001), Chan et al., (2002), Chan et al., (2003), Akkaya, (2007)].

The voltage loss associated with the gas transport of hydrogen and oxygen in an SOFC is caused by the concentration disparity between the reaction sites and the bulk [Akkaya, (2007)]. When the current draw is increased until the reaction sites are completely void of reactants, the limiting current density is reached. The limiting current densities are determined via the mass transport models described above (FM or DGM). The following expressions are used to characterize the concentration losses in SOFCs as a function of the limiting current density [Chan et al., (2001), Akkaya, (2007), Ivanov, (2004), Yoon et al., (2007)]:

$$V_{conc}^{an} = \frac{RT}{n_e F} \ln\left(\frac{1 - \frac{i}{i_{L,H_2}}}{1 + \frac{i}{i_{L,H_2O}}}\right) \tag{1.20}$$

$$V_{conc}^{ca} = \frac{RT}{n_e F} \ln\left(\frac{1}{1 - \frac{i}{i_{L,O_2}}}\right) \tag{1.21}$$

where V_{conc} are the anodic and cathodic losses respectively and the i_L's are the limiting current densities for each of the species.

1.3 Stack and System level SOFC modeling

The use of zero or 1D single cell electrochemical and mass transport models coupled with 1D or thermodynamic energy balances was the most common approach to stack level modeling in literature [Braun et al., (2005), Krumdieck et al., (2004), Chan et al., (2003), Zhang et al., (2003) , Lisbona et al., (2007), Padulles et al., (2000), Tanaka et al., (2000), Wu et al., (2008), Bavarsad (2007)]. These models were all single cell, with the results then being multiplied by the number of cells in the stack. The approach is difficult to evaluate as unit cell results were compared to unit cell data. A more appropriate method would be to compare unit cell results multiplied by the number of cells to stack level data. Padulles et al. (2000) evaluated the ohmic losses in terms of the entire stack; however, no details regarding the methodology used in determining those losses were included in the paper. Many of the stack models evaluated were part of larger system level models. For this reason the "average cell" approach is attractive as it simplifies the model. It is however, unlikely that no voltage loss or current drop would occur at the stack level compared to the individual cell. At the very least temperature distribution within the stack could affect the individual cell performance. Non uniform temperature within the cells has been considered at the stack level [Locket et al., (2003)]. A 3D simulation using FEM and CFD was conducted in this study to evaluate the temperature distribution and thermal stress within the stack. Results from this work however, were only used in stack design optimization.

System level models incorporate the SOFC stack as well as the internal reformer, and BOP components. BOP components can include compressors, blowers, burners, and depending on the type of system power conditioning units, turbines, or even addition fuel cells (PEM). In the literature reviewed the SOFC system was modeled as thermodynamic control volumes coupled with a black box equation [Zink et al., (2007), Hawkes et al. (2007)], zero-dimensional or 1D stack model. A control volume analysis is favourable for system level modeling for a couple reasons. First because, detailed information regarding temperature and species breakdown within the SOFC or BOP is not desired; only component performance for sizing, technology comparison and economic evaluation is. Secondly, if a 2D or 3D cell or stack model were to be used then models of similar order would need to be used for all system components for the system model to be considered 2D or 3D. A system level model of this magnitude would be cumbersome, time consuming to run and require much input data and knowledge about the system.

System level models have been incorporated into commercial and open source application software such as AspenPlus^{TM} [Lisbona et al., (2007)], ESP-r, and TRYNSYS. SOFC system level models incorporated into Software can be used to determine how an SOFC may interact with the electricity grid, or the building it is providing thermal energy too. Improving upon such model platforms is the purpose of the current research.

1.4 Research Objectives

The Annex 42 model currently provides a complete model framework which can be calibrated to any SOFC system given experimental data. However, the model can not evaluate changes to operating parameters such as fuel utilization, excess air ratio, or stack temperature. The model also can not be used to evaluate hypothetic systems or adjustments to a current design, such as, number of cells, electrode thickness, material, or cell diameter. The aim of the current research is to improve the treatment of the FCPM such that changes to operating parameters or even a hypothetical system can be tested within the framework of ESP-r. This main goal will be reached by the completion of the following research objectives;

1) Develop a semi-mechanistic model of the fuel cell stack. This model will be zero dimensional. The model will incorporate techniques as described in the above literature review.
2) Develop an appropriate energy balance of the fuel cell. The main purpose of the energy balance will be to evaluate the temperature of the fuel cell and regulate temperature through the use of the stack burner.
3) Calibrate and validate of the new FCPM model using existing experimental data.
4) Demonstrate the improved model's capabilities.

Chapter 2

Methodology

The current research is focused on the Annex 42 SOFC cogeneration model. This chapter will first provide an overview of the simulation code ESP-r used in this study, and then focus on the methodology of the new model representing the FCPM. The empirical relation currently implemented in ESP-r for electrical efficiency will be redefined in terms of the zero-dimensional cell model and improved FCPM energy balance. Subsequently, each aspect of the electrochemical and thermodynamic model will be derived.

2.1 Overview of ESP-r

The model developed in this thesis was implemented into the ESP-r simulation code. The overall structure of the ESP-r code and the SOFC cogeneration *system* therein are described in this section prior to discussing the detailed methodology for modelling the SOFC *stack*.

ESP-r is an environmental and energy-use building simulation program. ESP-r is a design tool for engineers, researcher and consultants alike. The objectives of ESP-r are to model the built environment is such a way that “a) is realistic and adheres closely to actual physical systems, b) supports early-through-detailed design stage appraisals, and c) enables integrated performance assessments in which no single issue is unduly

prominent." (http://www.esru.strath.ac.uk/Programs/ESP-r_overview.htm). ESP-r utilizes the finite-volume approach to solve the conservation equations specified by the user, in a domain (CAD) in an iterative time step method. Climate, occupant information and control strategies can also be analyzed in ESP-r.

The Annex 42 model which has been implemented in ESP-r uses 12 control volumes to represent two fuel cell cogeneration system configurations: one uses an SOFC and the other a proton exchange membrane (PEM) fuel cell. The current research is focused on the SOFC system which uses nine of the 12 control volumes. Those control volumes are [Kelly and Beausoleil-Morrison, (2007)]:

- Fuel cell power module
- Air supply blower
- Fuel supply compressor
- Water pump (if required for steam reformation)
- Auxiliary burner (if present upstream of the exhaust-gas-to-water heat exchanger)
- Exhaust-gas-to-water heat exchanger
- Battery system (for electrical storage)
- PCU (for converting the fuel cell's DC electrical output to AC)
- Air dilution system with optional heat recovery ventilator (HRV)

The focus of the current research is an improved FCPM model that is more generally applicable than the existing empirical representation. The FCPM consists of the stack and stack burner, as well as the balance of plant (BOP) components, including the fuel pre-heater and pre-reformer, the air pre-heater, after-burner, and fuel desulphurizer. In the

Annex 42 model, the FCPM must output the fuel/air/exhaust flow rates and temperature as well as its electrical efficiency. The exhaust gas information is used to estimate the performance of the heat exchanger that provides heat to the residential building. The electrical efficiency is used along with the input power required by the PCU (P_{el}) to determine the molar flow rates of the air and fuel as well as the power requirements of different system components represented by the other control volumes.

2.2 FCPM Electrical Efficiency

The Annex 42 model calculates the FCPM electrical efficiency using an empirical equation. This equation was calibrated using a series of seven experiments performed by NRCan on the FCT system in 2005 [Kelly and Beausoleil-Morrison, (2007)]. Further experiments conducted during the same time period were used to validate the results. The equation is as follows:

$$\eta_{FCPM} = (\varepsilon_0 + \varepsilon_1 P_{el} + \varepsilon_2 P_{el}^2)\left[1 - N_{stop} D\right]\left[1 - MAX\left|\int_0 t - t_{threshold}, 0\right| L\right] \qquad (2.1)$$

where the $[1 - N_{stops}D]$ term in Equation 2.1 represents the degradation of the electrical efficiency of the FCPM as a result of stop-start cycling. Due to high operating temperatures and the thermal stresses that may be experienced during system cool-down and warm-up periods, the fuel cell electrical performance will degrade with time. N_{stops} represents the number of times the SOFC cogeneration system has been stopped and then restarted and D is a user-input fixed value representing the fractional performance degradation associated with each cycle.

The "L" term in Equation 2.1 represents the degradation of the electrical efficiency of the FCPM as a result of operation time. L is a user-input fixed value representing the fractional performance degradation associated with operating time. The time integral represents the accumulated operation time from the initial system start. $t_{threshold}$ is a user-input fixed time value which can be used to represent systems that may show no degradation for a period of time ($t_{threshold}$), but degrade thereafter.

The ε_i coefficients in Equation 2.1, were deduced from the previously mentioned seven experiments performed by NRCan. However, it should be noted that these coefficients were obtained using average results from each of the experiments. The methodology of the NRCan experiments included an attempt to maintain the power draw of the FCPM to within 100 W of the target to mimic steady state operation. At the end of the experiments, an average power and fuel consumption were determined and the coefficients for Equation 2.1 were calibrated to those results.

The electrical efficiency calculated in Equation 2.1 is then used to determine the Fuel flow rate to the FCPM such that:

$$\dot{N}_{fuel-FCPM} = \frac{P_{el}}{\eta_{FCPM} LHV_{fuel}} \tag{2.2}$$

where $\dot{N}_{fuel\text{-}FCPM}$ is the fuel flow rate (kmol·s^{-1}) to the FCPM and LHV_{fuel} is the lower heating value (J·kmol) of the fuel. The fuel flow rate includes the fuel for the SOFC stack and the fuel for the stack burner. The stack burner is used to maintain the temperature within the stack.

2.3 Improvements to the Treatment of the FCPM Electrical Efficiency

With the method for calculating FCPM efficiency by the Annex 42 model shown, the improvements to the model can be presented. The proposed model is a zero-dimensional cell model coupled with a thermodynamic energy balance. This model is coded in FORTRAN and then implemented into ESP-r, within the existing Annex 42 model framework. The zero-dimensional model and the level of details in representing the physical processes were selected keeping in mind the integration with the overall code and also to facilitate the calculation and transfer of non-dimensional and physical parameters (i.e. efficiency, gas temperature, etc.). A review of current literature presented in Chapter 1 also demonstrated that zero-dimensional representation is appropriate for system level modeling. The proposed model requires little computational effort which aids in reducing the time requirement for longer (year-scale) simulations.

In the proposed model, the fuel flow rate to the fuel cell stack (FCS) and the stack burner are calculated separately as opposed to using a lumped parameter for both in Equation 2.2. The FCS fuel flow rate will be determined based on the FCS efficiency. The FCS efficiency will be calculated using a zero-dimensional electrochemical model. This zero-dimensional model will be semi-mechanistic and based on the literature described in Chapter 1. The fuel flow to the stack burner will be determined based on the results of the fuel cell energy balance presented in Section 2.4. The fuel flow rate to the FCS can be defined in terms of its efficiency:

$$\dot{N}_{fuel-stack} = \frac{P_{stack}}{\eta_{FCS} LHV_{fuel}} \tag{2.3}$$

where η_{FCS} is the efficiency of the fuel cell stack and P_{stack} is the outputted power (W) of the stack. The stack power is defined as:

$$P_{stack} = P_{el} + P_{dc,ann} \tag{2.4}$$

where $P_{dc,ann}$ represents the parasitic power (W) draw of the BOP components as well as the voltage drop between the stack and the power conditioning unit (PCU).

Finally, the FCPM efficiency can be defined in terms of the fuel flow terms:

$$\eta_{FCPM} = \frac{P_{el}}{(\dot{N}_{fuel-stack} + \dot{N}_{fuel-burn})LHV_{fuel}} \tag{2.5}$$

where $\dot{N}_{fuel\text{-}stack}$ and $\dot{N}_{fuel\text{-}burn}$ are the fuel requirements (kmol·s^{-1}) of the fuel cell stack and the stack burner, respectively. The following section presents the BOP component analysis, the improved semi-mechanistic model and energy balance for the FCPM.

2.3.1 Balance of Plant

The BOP component power draw must be determined in order to evaluate the total power required from the fuel cell stack. The BOP components include the fuel desulphurizer and pre-heater, the air filter and pre-heater, and the after burner. The exact types and arrangement for the BOP components is proprietary knowledge for the FCT system. There are a number of different possible configurations, and Figure 1.1 presents one possibility. The current design of the FCT system had a substantial voltage loss between the FCS and the PCU. This voltage drop is considered in the proposed model and is incorporated within the BOP power draw ($P_{dc,ann}$). An empirical correlation has been

developed to describe $P_{dc,ann}$. The equation was calibrated using data collected during the NRCan experiments as presented in Figure 2.1. Since the proposed model must be capable of representing the FCT system and no information was available regarding the BOP components for that system, the use of an empirical correlation was necessary for this portion of the model. An exponential form was chosen because it ensures that a minimum value will be assigned to the power consumption even at low P_{el} values. The exponential form also gave the best R^2 representation of the NRCan data. The following equation is used to determine $P_{dc,ann}$:

$$P_{dc,ann} = P_{dc,comp} + P_{IV} = \varepsilon_{ann-o} e^{\varepsilon_{ann-1} P_{el}} + \varepsilon_{IV-o} e^{\varepsilon_{IV-1} P_{el}} \quad (2.6)$$

where $P_{dc,\,comp}$ is the power (W) draw of the BOP components *and* P_{IV} is the power (W) loss due to the ohmic losses between the stack and the PCU. The ε terms represent the empirical constants, as shown in Table 2.1. The ε terms correlated well with the experimental results with R^2 values for the power loss due the voltage drop and the DC,ann draw of 0.98 and 0.88, respectively.

Equation 2.6 can also be generalized in order to test hypothetical systems:

$$P_{dc,ann} = \sum_i P_i(n_1, n_2 \ldots) \quad (2.7)$$

where *i* represents the hypothetical BOP component, and *n* represents the variable of which *i* is a function. For example, power to the air supply blower would be a function of the pressure change and air flow rate. The values presented in Table 2.1 as well as the previous form of the $P_{dc,ann}$ equation are only applicable to the FCT device.

Table 2.1 Coefficients used to determine $P_{dc,ann}$ (Equation 2.6). These coefficients were generated from the NRCan experimental data presented in Figure 2.1.

Coefficient	Value	Unit
ε_{ann-o}	144.22	W
ε_{IV-o}	7.9764	W
ε_{ann-1}	0.00037	W^{-1}
ε_{IV-1}	0.00097	W^{-1}

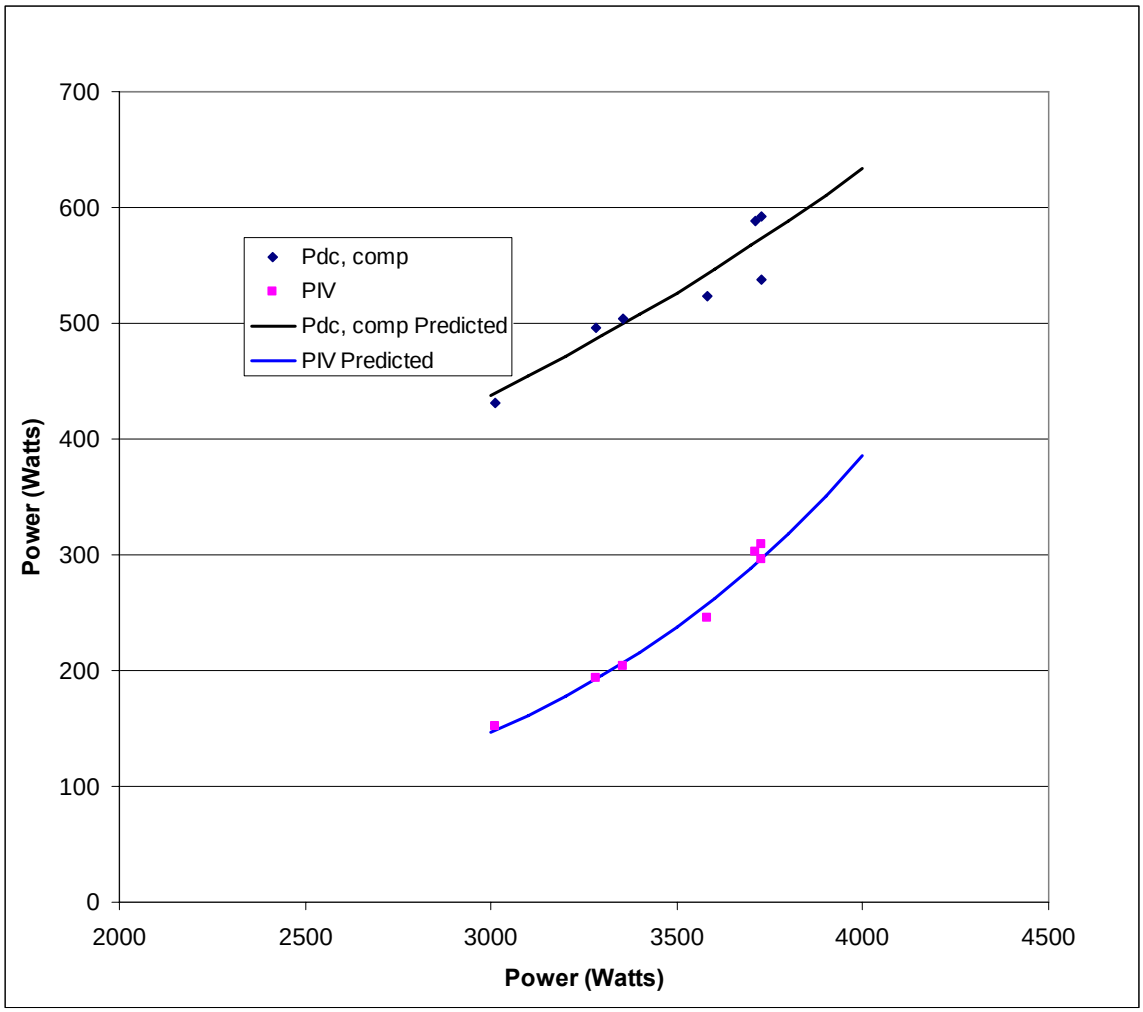

Figure 2.1 NRCan experimental results for DC ancillary draws of the FCPM BOP components and power loss due to voltage drop between the FCPM and the PCU plotted against P_{el}. Results for the two losses as a function of P_{el} predicted by the model using Equation 2.6 and the values in table 2.1.

2.3.2 Fuel Cell stack

Once the stack power (P_{stack}) has been evaluated, it can be used to determine the stack current and voltage. P_{stack} is a function of the stack voltage and current such that:

$$P_{stack} = n_{cells-parrallel} I_{cell} n_{cells-series} V_{cell} \tag{2.8}$$

where $n_{cells\text{-}parallel}$ and $n_{cells\text{-}series}$ are the number of cells in parallel and series in the fuel cells stack arrangement, respectively, and I_{cell} and V_{cell} are the current (A) and voltage (V) of a single cell. V_{cell} can be expressed as the Nernst voltage minus losses due to current draw. Within the model, activation polarization, ohmic losses and concentration polarization are considered, such that:

$$V_{cell} = E_r - V_{act} - V_{ohm} - V_{con} \tag{2.9}$$

where E_r is the Nernst reversible voltage (Equation 1.15) (V), V_{act} is the activation polarization, V_{ohm} is the ohmic loss, and V_{con} is the concentration polarization (V) of each cell. The model assumes that all reactant gases behave ideally, and that the operating pressure is 1 bar. The polarization losses in Equation 2.9 can be predicted via known electrochemical and mass transfer techniques reported throughout the literature [Larminie and Dicks, (2002), Akkaya, (2007), Chan et al., (2001), Yoon, (2007), Campanari, 2004, Sanchez 2008, Bessette et al., (1995), Kim et al., (1999) , Singhal and Kendall, (2004)], and as described below.

2.3.2.1 Reformation of methane and other hydrocarbon fuels

In order to evaluate the Nernst potential the partial pressure of hydrogen, oxygen and water is required. The activation and concentration polarization terms in Equation 2.9

also require the partial pressures of the gases as inputs. Therefore, the partial pressures of all gases as they enter the SOFC must be determined. If hydrogen or carbon monoxide is used as fuel, the partial pressures are easily determined as both hydrogen and carbon monoxide will react directly in an SOFC. However, other hydrocarbons such as methane must first be reformed into hydrogen and carbon monoxide before they can generate electricity in an SOFC. Therefore, the reformation reactions must be considered when deriving the partial pressures of hydrogen, carbon dioxide and other gases when methane (or other hydrocarbons) are used as SOFC fuel. In Chapter 1 the equations describing reformation were given (Equations 1.2-4).

The proposed model assumes that reaction 1.2a and 1.2b are complete, i.e. all of the methane or unspecified hydrocarbon reforms. The justification for this assumption must be considered for two cases: first, if methane is the fuel and second, if another hydrocarbon is chosen. Reformation models developed by [Sanchez et al., (2008), Campanari and Iora, (2004), Nehter, (2006)] found that the methane completely reforms within the first third of the SOFC tube length. Since the scale of this model is zero-dimensional, it is reasonable to assume that Equation 1.2a is complete. For the case where a generic hydrocarbon is used as fuel, the assumption is made for the sake of simplicity. Any hydrocarbon other then methane would likely require external reformation. Reformation is represented by a complex set of equations and rate limiting steps that are different for each fuel chosen. It is beyond the scope of this work to try and accommodate each possible hydrocarbon. Caution should therefore be exercised if the model is applied when another hydrocarbon is used.

For the purpose of solving the gas shift reaction (Equation 1.10) methane will be assumed as the fuel. With complete reformation of methane, the value of (x) in Equation 1.10 is equal to the initial molar flow rate of methane. With this simplification, (y) or the molar flow rate of CO that reacts with water to form hydrogen and carbon dioxide, can be determined. MATLab was used to derive a symbolic solution to the non-linear gas shift Equation 1.10. This equation is cumbersome and therefore included as Appendix A.

where U_f is the fuel utilization. From Equations 1.8 and Appendix A, we can determine the mole fraction of each constituent:

$$\chi_{H_2O} = \frac{(H_2O^i - CH_4^i - y + U_f(3CH_4^i + y)}{(H_2O^i + 3CH_4^i)};$$
$$\chi_{H_2} = \frac{(3CH_4^i + y - U_f(3CH_4^i + y)}{(H_2O^i + 3CH_4^i)}; \qquad (2.10)$$
$$\chi_{CO_2} = \frac{CO_2^i + y}{(H_2O^i + 3CH_4^i)}; \chi_{CO} = \frac{CO^i + x - y}{(H_2O^i + 3CH_4^i)}$$

Finally, assuming ideal gases and a system pressure of 1 bar, the partial pressures of each gas are equal to their mole fraction and actual pressure. The partial pressures derived in this section are used in both the Nernst potential calculation and cell polarization as described below.

2.3.2.2 Activation Polarization

The electrochemical reaction in the fuel cell requires a certain amount of energy to proceed. The voltage loss associated with this process (V_{act} in Equation 2.9), is characterized by the Butler-Volmer equation (Equation 1.16). Equation 1.16 can be

applied to both the anode and cathode reactions. In order to solve Equation 1.16, the proposed model assumes $\beta = 0.5$, then:

$$\frac{i}{i_O} = e^{\left(\frac{0.5\, n_{eFV\ act}}{RT}\right)} - e^{\left(\frac{-0.5\, n_{eFV\ act}}{RT}\right)} = e^{\left(\frac{0.5\, n_{eFV\ act}}{RT}\right)} - \frac{1}{e^{\left(\frac{0.5\, n_{eFV\ act}}{RT}\right)}} \tag{2.11}$$

Multiplying both sides by $e^{\left(\frac{0.5 n_{eFV_{act}}}{RT}\right)}$ allows for a quadratic equation of the form:

$$e^{\left(\frac{0.5 n_{eFV_{act}}}{RT}\right)^2} - \frac{i}{i_O} e^{\left(\frac{0.5 n_{eFV_{act}}}{RT}\right)} - 1 = 0 \tag{2.12}$$

Applying the quadratic formula, the following equation is obtained:

$$V_{act} = \frac{2RT}{n_e F} \ln\left(\frac{i}{i_O} + \sqrt{\frac{i}{i_O}^2 + 4} \right) \tag{2.13}$$

Recognizing this as the inverse hyperbolic arcsine, the anode and cathode activation over-potentials can be expressed as [Yoon et al., (2007)]:

$$V_{act}^{an} = \frac{2RT}{n_e F} \sinh^{-1}\left(\frac{i}{2i_{o,an}} \right) \tag{2.14}$$

$$V_{act}^{ca} = \frac{2RT}{n_e F} \sinh^{-1}\left(\frac{i}{2i_{o,ca}} \right) \tag{2.15}$$

where the super/subscripts *an* and *ca* stand for the cathode and anode side reactions, respectively. The exchange current density (i_o) ($A \cdot cm^{-2}$) is then the only parameter remaining to be determined. The exchange current density can be expressed using Equation's 1.17 and 1.18.

2.3.2.3 Ohmic Losses

Ohmic losses are caused by the resistivity of the SOFC materials to current-flow. To determine the Ohmic losses (V_{ohm} in Equation 2.9), the proposed model employs an equivalent resistance [Yoon 2007, Krumdieck et al., (2004), Padulles et al., (2000), Chan et al. (2001), Akkaya, (2007)] and then applies Ohm's Law.

$$V_{ohm} = iR_{eq} \tag{2.16}$$

where R_{eq} is the area specific equivalent resistance (ohm·cm^2) of the cell.

The equivalent resistance is presented in Figure 2.2. Nisancioglu (1989) has developed an analytical solution to the equivalent resistant of a tubular SOFC [Nisancioglu, (1989)]. This solution is used by the proposed model with corrections for the temperature dependence of conductivity. The following equations are used to evaluate the equivalent resistance:

$$R_1 = \frac{\left[\left(\frac{1}{\sigma_{an}L_{an}}\right)^2 + \left(\frac{1}{\sigma_{ca}L_{ca}}\right)^2\right]\cosh(Z_e) + \left(\frac{1}{\sigma_{an}L_{an}\sigma_{ca}L_{ca}}\right)\left(2 + Z_e\sinh(Z_e)\right)}{2\left(\frac{\sigma_{el}}{L_{el}}\right)^{1/2}\left(\frac{1}{\sigma_{an}L_{an}} + \frac{1}{\sigma_{ca}L_{ca}}\right)^{3/2}\sinh(Z_e)} \tag{2.17a}$$

$$Z_e = \frac{Path_{el}}{2}\sqrt{\left(\frac{\sigma_{el}}{L_{el}}\right)\left(\frac{1}{\sigma_{an}L_{an}} + \frac{1}{\sigma_{ca}L_{ca}}\right)} \tag{2.17b}$$

$$R_{\text{int}} = \frac{L_{\text{int}}}{\sigma_{\text{int}}A_{\text{int}}} \tag{2.17c}$$

$$R_{eq} = \frac{R_1 A_{cell}}{L_{cell}} + R_{\text{int}}A_{cell} \tag{2.17d}$$

where the subscripts *el* and *int* stand for electrolyte, and interconnect, respectively, L is the layer thickness(cm), σ is the conductivity ($\Omega^{-1}\cdot cm^{-1}$) of the material, and A is the area (cm^2) perpendicular to current flow. L_{cell} refers to the length of the entire cell and $Path_{el}$ is radial distance (circumference) (cm) of the electrolyte.

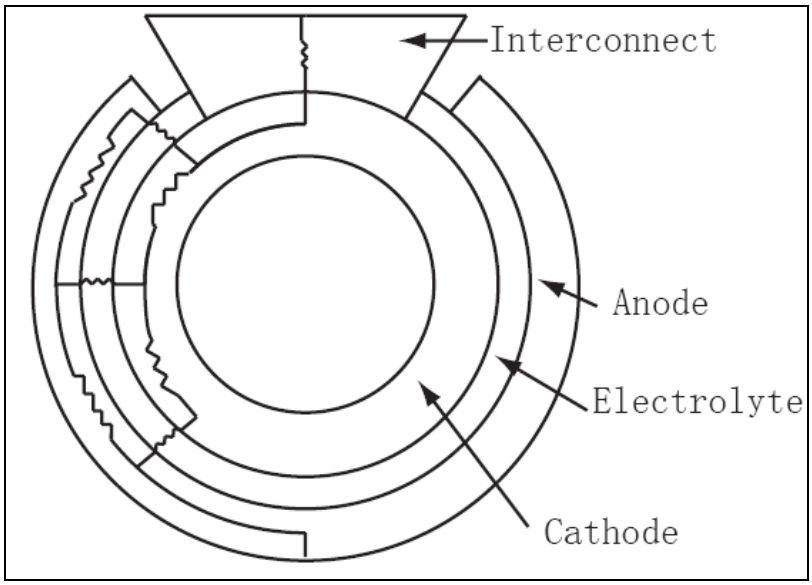

Figure 2.2 Equivalent resistance circuit for a single SOFC tube.

2.3.2.4 Concentration Polarization

Concentration polarization is the voltage loss due to the limitations of diffusive transport of gases to the reaction sites (V_{con} in Equation 2.9). As discussed in Chapter 1, the equations that describe the anode and cathode concentration losses are:

$$V_{con}^{an} = \frac{RT}{n_e F}\ln\left(\frac{1-\frac{i}{i_{L,H_2}}}{1+\frac{i}{i_{L,H_2O}}}\right) \tag{2.18}$$

$$V_{con}^{ca} = \frac{RT}{n_e F}\ln(1-\frac{i}{i_{L,O_2}}) \tag{2.19}$$

where $i_{L,I}$ is the limiting current density ($A \cdot cm^{-2}$) of the reaction gases. The limiting current density for each species can be determined using the fundamental equation for isothermal transport of gaseous species in porous electrodes [Kim et al., (1999)]. At the anode, hydrogen and the water diffuse in opposite directions with the same flux. The equations describing each gas are:

$$J_{H_2} = -D_{H_2,eff}\nabla c_{H_2} + \chi_{H_2}\delta_{H_2}J_{tot} - \chi_{H_2}\gamma_{H_2}\left(\frac{cB_o}{\mu}\nabla P\right) \tag{2.20}$$

$$J_{H_2O} = -D_{H_2O,eff}\nabla c_{H_2O} + \chi_{H_2O}\delta_{H_2O}J_{tot} - \chi_{H_2O}\gamma_{H_2O}\left(\frac{cB_o}{\mu}\nabla P\right) \tag{2.21}$$

where J_{H2O} and J_{H2} are the molar fluxes of each species, D_{eff} is the effective diffusion coefficient ($cm^2 \cdot s^{-1}$), c is the concentration χ is the mole fraction, δ is the ratio of Knudsen to total diffusion and J is the total molar flux ($mol \cdot cm^{-2} \cdot s^{-1}$). The final term in both equations is a convective transport term. Convective transport is not considered in this work because pressure change within the pores is assumed to be negligible [Suwanwarangkul et al., (2003)]. Nevertheless, γ is the ratio of binary to total diffusion, B_o is the permeability, μ is the viscosity ($g \cdot cm^{-1} \cdot s^{-1}$) and P is the pressure (bar). The total diffusion flux J will be zero since the molar diffusion of hydrogen and water are equal at steady state and J is their sum. Equations 2.20 and 2.21 can be further simplified by assuming one-dimensional transport, the ideal gas law and the relationship between current and molar flux (Equation 2.23). Also, in this analysis, hydrogen will be examined; the same argument holds for water as well:

$$\frac{dc_{H_2}}{r} = \frac{dP_{H_2}}{L_{an}RT} \tag{2.22}$$

$$J_{H_2} = -\frac{i}{2F} \tag{2.23}$$

where L_{an} (cm) is the thickness of the anode electrode. Equation 2.20 simplifies to:

$$i = \frac{D_{eff,H_2}\, 2F(P^I_{H_2} - P_{H_2})}{RTL_{an}} \tag{2.24}$$

where P^I_{H2} denotes the initial or the bulk pressure (bar) of the gas. Considering that the limiting current density is reached when the partial pressure at the reaction sites approaches zero, the limiting current densities for hydrogen and water are:

$$i_{L,H_2} = \frac{n_e F D_{eff,H_2}}{RTL_{an}} P_{H_2} \tag{2.25}$$

$$i_{L,H_2O} = \frac{n_e F D_{eff,H_2O}}{RTL_{an}} P_{H_2O} \tag{2.26}$$

For the case of oxygen in air, the net flux of nitrogen is zero [Chan et al., (2001)], therefore the governing diffusion equation is:

$$J_{O_2} = -D_{O_2}\nabla n_{O_2} + \chi_{O_2}\delta_{O_2} J_{O_2} \tag{2.27}$$

Again assuming one-dimensional diffusion, ideal gas law, the relationship between molar flux and current as well as the definition of mole fraction, this equation simplifies to:

$$i = \frac{D_{eff,O_2}\, 4F(P^I_{O_2} - P_{O_2})}{RTL_{ca}(1 - \frac{P_{O_2}}{P_T}\delta_{O_2})} \tag{2.28}$$

where L_{ca} is the cathode thickness (cm) and P_T is the total pressure (bar) at the cathode. Given that the total cathode side pressure is assumed to be 1 bar and the limiting current

density occurs when the oxygen pressure nears zero at the reactant site, the limiting current density is:

$$i_{L,O_2} = \frac{n_e F D_{eff,O_2}}{RTL^a(1 - P_{O_2}\delta_{O_2})} P_{O_2} \tag{2.29}$$

In order to evaluate Equations 2.25, 2.26 and 2.29 the effective diffusion coefficients for each species must be determined in ($cm^2 \cdot s^{-1}$). The effective diffusion coefficient for each species is calculated using binary and Knudsen diffusion coefficients. The methods described by Todd (2002), are used for the binary diffusion coefficients and the Knudsen is expressed through an equation relating the mean-free path to average pore size such that (hydrogen used as example) [Chan et al., (2001), Todd, (2002)]:

$$\frac{1}{D_{eff,H2}} = \frac{\varepsilon}{\tau}\left(\frac{1}{D_{H2,k}} + \frac{1}{D_{H2,H2O}}\right) \tag{2.30}$$

$$D_{H2-H2O} = \frac{0.00143T^{1.75}}{M_{H2-H2O}^{1/2}(\nu_{H2}^{1/3} + \nu_{H2O}^{1/3})^2 P} \tag{2.31}$$

$$D_{H2,k} = 97.0 r_{por}\sqrt{\frac{T}{M_{H2}}} \tag{2.32}$$

where ε is porosity, τ is tortuosity, M is molar mass ($kg \cdot kmol^{-1}$), ν is diffusion volume (cm^3) and r_{por} is the pore length (cm). Given a current density, Equations 2.18 and 2.19 can now be used to determine the concentration polarization losses at the cathode and anode.

2.3.2.5 Stack Resistance

The proposed model thus far has been limited to the cell level polarization and has not considered the coupling of the cells into the stack. Dynamic effects have also not been modelled. There is little research available in the literature dedicated to modelling entire stacks beyond the expedient and simplistic approach of multiplying a cell voltage by the number of cells in the stack [Braun et al., (2005), Krumdieck et al., (2004), Chan et al., (2003), Zhang et al., (2003) , Lisbona et al., (2007), Padulles et al., (2000), Tanaka et al., (2000), Wu et al., (2008), Bavarsad (2007)]. In order to account for the additional losses observed in excess of the sum of the individual cell losses, the current model proposes an additional voltage loss termed stack resistance voltage. The stack resistance occurs due to the connection of the cells together in series or parallel. The stack resistance is empirically determined. Introducing this additional voltage loss normalized to a single cell, V_{cell} is now:

$$V_{cell} = E_r - V_{act} - V_{ohm} - V_{con} - V_{SR} \tag{2.33}$$

where V_{SR} is the stack resistance voltage (V).

2.2.3.6 FCS Efficiency

Now that V_{stack} has been expressed as a function of the current density, it can be determined at any value of stack power. Considering V_{stack} and U_f, the efficiency of the stack can also be expressed as:

$$\eta_{stack} = \frac{V_{stack}}{E_h} U_f \tag{2.34}$$

where E_h is the theoretical maximum voltage (V) based on the LHV of the fuel, and η_{stack} is the stack efficiency. Finally, given the stack efficiency and P_{stack}, the fuel flow rate through the stack can be determined (Equation 2.3).

2.4 Temperature Model

Many of the parameters described in the preceding equations are temperature-dependent. In particular, due to the high sensitivity of conductivity to temperature, if the temperature in the stack drops substantially, then the voltage losses will increase and the system will not operate effectively. In the FCT system, the stack burner is used to control the temperature of the stack. In the new model, an energy balance is used to determine the temperature of the stack. If that temperature is not sufficient then the stack burner is switched on. In the model, this will correspond to the introduction of the second fuel flow rate term to the FCPM, $\dot{N}_{fuel\text{-}burn}$ (Equation 2.5). The new model operates in this way to mimic the FCT system; however, it can be adapted to another system with a different temperature control mechanism. In order to determine the temperature of the stack the FCPM must be sub-divided into the fuel cell stack control volume (FCV), as illustrated in Figure 1.1. The FCV contains the SOFC stack as well as the stack burner. The energy balance for this control volume is:

$$(MC_\rho)\frac{\partial T_{FCV}}{\partial t} = \dot{H}_{air} + \dot{H}_{fuel} - \dot{H}_{products} - P_{stack} - q_{skinlosses} \tag{2.35}$$

where MC_ρ is the thermal capacitance ($J \cdot K^{-1}$) of the FCV and T_{FCV} is the temperature of the fuel cell control volume. $\dot{H}_{air}$, $\dot{H}_{fuel}$ and $\dot{H}_{products}$ are the enthalpy flow rates ($J \cdot kmol^{-1} \cdot s^{-1}$) of the air entering, the fuel entering and the product gases leaving the FCV respectively. $\dot{H}_{products}$ includes the product H_2O vapour and CO_2 from the electrochemical reaction, the products of the combustion of the un-reacted fuel, and the excess air. Finally, $q_{skinlosses}$ are the heat losses (W) from the fuel cell stack to the surroundings.

In Equation 2.35, each of the enthalpy flows are equal to the summation of the enthalpies of the individual constituents such that:

$$\dot{H}_{air} = \sum_i (\dot{N}_i \hat{h}_i)_{air} \tag{2.36a}$$

$$\dot{H}_{fuel} = \sum_i (\dot{N}_i \hat{h}_i)_{fuel} \tag{2.36b}$$

$$\dot{H}_{products} = \sum_i (\dot{N}_i \hat{h}_i)_{products} \tag{2.36c}$$

where $\dot{N}_i$ is the molar flow rate in ($kmol \cdot s^{-1}$) and $\hat{h}_i$ is the molar enthalpy in ($J \cdot kmol^{-1}$) of an individual constituent within the air, fuel or products gases. The enthalpies in Equations 2.36a-c are standardized to a reference state to ensure that the compounds within the reactants and products are properly related to each other. The standard state is 1 bar and 25 °C.

The molar flow rate of the air stream in Equation 2.36a is determined by the stoichiometric requirements of the combustion reaction and the excess air ratio, λ_{air}, such that:

$$\dot{N}_{air\ stoic} = \frac{\dot{N}_{fuel-stack}}{2p_{O_2}} \tag{2.37}$$

$$\dot{N}_{air} = (1+\lambda_{air})\dot{N}_{air\ stoic} \tag{2.38}$$

where $\dot{N}_{airstoic}$ (kmol·s^{-1}) is the theoretical amount of O_2 required by the electrochemical reactions and p_{O2} is the partial pressure of the O_2 in the air stream. The molar flow rate of the fuel is determined by Equation 2.5 and the molar flow rate of the products by assuming complete combustion and electrochemical reaction of all the gases.

The temperature of each of the gases must also be known in order to determine the enthalpies. The temperatures of the gases as they enter the FCPM are known and described in detail in [Kelly and Beausoleil-Morrison 2007]; however, the temperatures of the fuel and product gases entering and leaving the FCV are not known. For the fuel and air, this is the temperature leaving the respective pre-heaters. The pre-heaters use the exhaust gases from the fuel cell as hot input streams. However, the exact configuration of these heat exchangers is proprietary knowledge. In the current research, an empirical relationship for the pre-heaters is proposed, in which the temperatures of the gases as they enter the FCV are given as a function of their temperatures as they enter the FCPM and as they exit the stack. In order to develop this relationship we must first consider an idealized heat exchanger for both the air and fuel pre-heaters as follows:

$$\begin{aligned}&(\dot{N}C_\rho)_{product}(T_{FCV} - T_{products-FCPM}) = \\ &(\dot{N}C_\rho)_i(T_{i,inFCV} - T_{i,inFCPM})\end{aligned} \tag{2.39}$$

Where $\dot{N}$ is the molar flow rate (kmol·sec^{-1}) and Cp is molar heat capacity (J·K^{-1}·mol^{-1}). The T_i terms represent temperature where the subscript definitions are as follows: *stack*

signifies the fuel cell stack, *products-FCPM* signifies the gases exiting the FCPM, and *i,inFCV* refer to either the fuel or air stream entering the fuel cell control volume. In the current work, the ratio of $\dot{N}C_p$ for the products and the gases (fuel and air) is used to develop two "heat exchanger effectiveness" parameters. Using these empirical values, we can determine the temperature of the air and fuel as they enter the FCV:

$$T_{i,inFCV} = \beta_i (T_{FCV} - T_{products-FCPM}) + T_{i,inFCPM} \tag{2.40}$$

where β_i is the heat transfer coefficient for the air and fuel. The β_i values can be determined from the heat transfer properties of the pre-heaters. In the event that these properties and configurations are not known, experimental data can be used (as was the case with the FCT system).

Finally, if assumptions of an isothermal stack temperature, complete combustions of all gases, and that the gases reach the stack temperature before exiting the stack, are made, then $T_{stack} = T_{products} = T_{FCV}$ = T (electrochemical reactions). The molar enthalpy of the products can now be evaluated at T_{stack}. Equation 2.35 can be re-written to include the abovementioned analyses as follows:

$$\begin{aligned}(MC_{\rho})\frac{\partial T_{FCS}}{\partial t} &= \sum_i (\dot{N}_i[\hat{h_i} - \Delta f \hat{h}^{\circ}_i])_{air} \\ &+ \sum_i (\dot{N}_i[\hat{h_i} - \Delta f \hat{h}^{\circ}_i])_{fuel} + \dot{N}_{fuel}\, LHV_{fuel} - \\ &\sum_i (\dot{N}_i[\hat{h_i} - \Delta f \hat{h}^{\circ}_i])_{products} - P_{stack} - q_{skinlosses}\end{aligned} \tag{2.41}$$

where $\Delta f\hat{h}_i^o$ is the standard enthalpy of formation ($J \cdot kmol^{-1}$). If the stack temperature drops below a certain threshold then the stack burner is turned on. The energy balance must in turn be modified to account for this additional energy flow:

$$(MC_\rho)\frac{\partial T_{FCS}}{\partial t} = \dot{H}_{air} + \dot{H}_{fuel} + \dot{H}_{stack-burn} - \dot{H}_{products} - P_{stack} - q_{skinlosses} \tag{2.42}$$

where $\dot{H}_{stack\text{-}burrn}$ is the enthalpy flow of the stack burner, equal to:

$$\dot{H}_{stack-burn} = \dot{N}_{fuel-burn}\left(LHV_{fuel} + \sum_i ([\hat{h}_i - \Delta f\hat{h}_i^\circ])_{fuel} - \sum_i ([\hat{h}_i - \Delta f\hat{h}_i^\circ])_{products-burn}\right) \tag{2.43}$$

where $\dot{N}_{fuel\text{-}burn}$ is the molar flow rate of the fuel entering the stack burner and *products-burn* refers to the CO_2 and H_2O released during the combustion of the fuel. The air required for the combustion of the stack burner fuel is already accounted for in the energy balance; as no additional air is added to the system in response to the burner being turned on. Once the burner is switched on, $\dot{N}_{fuel\text{-}burn}$ is held constant until the desired stack temperature is reached.

2.5 FCT Experimental Results

Data collected from the FCT experiments has been used to determine the energy storage or thermal capacitance of the FCV (MC_p). Data analyses of the NRCan experiments were chosen for the evaluation of MC_p because information regarding the materials and configuration of the entire stack was not available. For the experiment, the FCT fuel cell system and BOP components were shut down after a period of steady operation and allowed to cool. Temperature measurements of the FCS were then recorded during the

cooling process. A lumped-capacitance energy analysis was applied to the experimental data: a lumped-capacitance method was chosen because the arrangement and materials of all system components were not known. The lack of knowledge surrounding the components made lumped capacitance a convenient approach. The approach was validated by applying the theory to the data; as shown in Figure 2.3, the R^2 value was over 0.99. Lumped capacitance can be derived from the energy equation:

$$\dot{E}_{in} + \dot{E}_{g} - \dot{E}_{out} = \frac{dE_{st}}{dt} = \dot{E}_{st} \tag{2.44}$$

where $\dot{E}_{in}$, $\dot{E}_{g}$, $\dot{E}_{out}$, and $\dot{E}_{st}$ are the energy (W) into, generated, out of and stored within the system, respectively. When the FCT system cools, there is no generation of energy or energy flow into the system. Therefore, Equation 2.44 reduces to:

$$-\dot{E}_{out} = \dot{E}_{st} \tag{2.45}$$

or

$$-(UA)_{eff}(T - T_{amb}) = MC_{p}\frac{dT}{dt} \tag{2.46}$$

where $(UA)_{eff}$ is the is the heat loss coefficient ($W \cdot K^{-1}$) for radiation and convection, T is the temperature (K) of the FCS and T_{amb} is the ambient temperature (K). By redefining temperature in terms of a temperature difference term, DeWitt (2002) evaluated Equation 2.44 as follows:

if

$$\theta = T - T_{amb} \tag{2.47}$$

then

$$\frac{d\theta}{dt}\frac{MC_p}{(UA)_{eff}} = -\theta$$

Using separation of variables and integrating with initial conditions $t = 0$ and $T(0) = T_I$:

$$\frac{MC_p}{(UA)_{eff}}\int_{\theta_i}^{\theta}\frac{d\theta}{\theta} = -\int_0^t dt$$

where

$$\theta_I = T_I - T_{amb} \tag{2.48}$$

Evaluating the integral gives the general form of lumped-capacitance method for the cooling FCT system:

$$\frac{\theta}{\theta_I} = \exp\left(-\frac{t}{\tau_t}\right) \tag{2.49}$$

where τ_t is the time constant of the system, and t is the time (s). τ_t is defined as such:

$$\tau_t = \frac{MC_p}{(UA)_{eff}} \tag{2.50}$$

Figure 2.3 presents a plot of the ratio θ / θ_i vs. time for the NRCan experiment. Equation 2.49 can be applied to the curve to determine the time constant, which is approximately 29000 s.

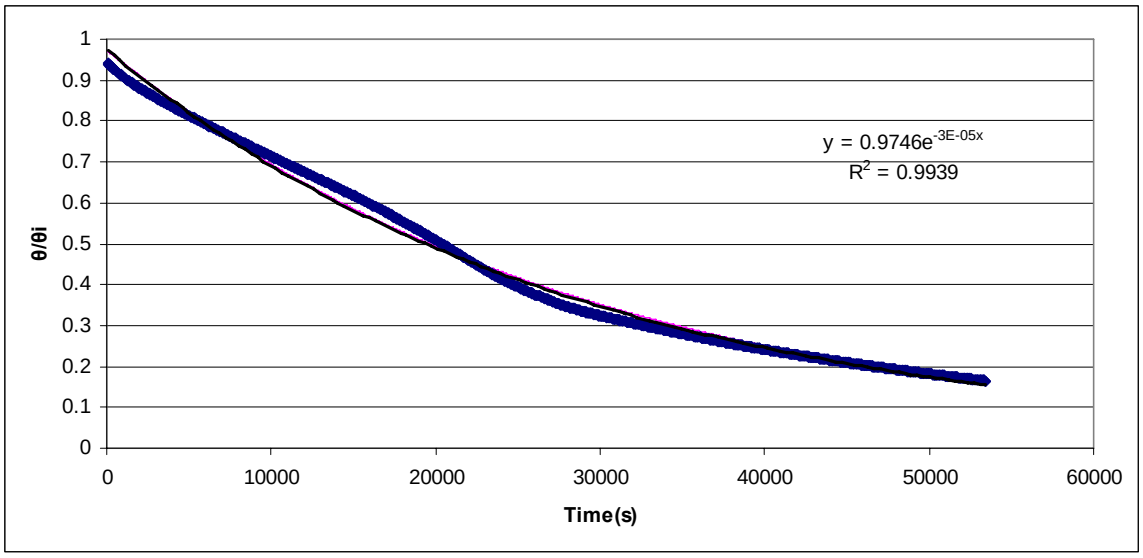

Figure 2.3 Temperature degradation in the SOFC stack vs. time for the FCT system when it was allowed to cool. The data was collected by NRCan. The exponential equation used to derive the time constant is also presented along with its R^2 value.

The cooling of the FCT system is due to energy transfer Q_{LC} to the surroundings. Q_{LC} can be evaluated as described by DeWitt (2002), given that:

$$Q_{LC} = \int_0^t q_{LC}\,dt = (UA)_{eff} \int_0^t \theta dt \tag{2.51}$$

and by substituting equation 2.50 into 2.52, the following equation can be obtained:

$$Q_{LC} = (MC_p)\theta_i \left[1 - \exp\left(-\frac{t}{\tau_t}\right)\right] \tag{2.52}$$

Having obtained this expression using the lumped capacitance method, we need to determine MC_p. In order to calculate MC_p, Equation 2.52 can be substituted into Equation 2.35. Temperature results from the NRCan experiments can be used to then determine MC_p for the FCV using this method.

Chapter 3

Simulation and Validation Results

Chapter 2 outlined the methodology used to generate the improved FCPM model. In this chapter an analyses of the results provided by the model as implemented in ESP-r is presented. First an examination of the predicted polarization losses at the cell level is given. The cell results also are compared to data from Singhal and Kendall (2004). Then stack level results are compared to the NRCan experimental results. The discrepancy between the cell and stack level predictions is also considered by analysing both the Singhal and Kendall (2004) and NRCan data. Following this, the complete improved FCPM model is examined, including the stack resistance, and the energy balance. ESP-r is used to compare results from the improved model to NRCan experimental data. Finally the new capabilities provided by the model are demonstrated as they pertain to operating conditions which can be controlled; namely, U_f, excess air ratio, and set point temperature.

3.1 Single Cell Model Results

As described in Chapter 2 there are three main losses which affect the cell voltage cell: 1) activation, 2) ohmic and 3) concentration polarization. Figure 3.1 presents those losses as a function of current density using the model described in the previous chapter. For this analyses cell temperature was set to1245 K and the fuel was methane at an U_f of 0.75. The activation losses are the largest followed by ohmic and then concentration (Figure

3.1). The exponential expansion of the concentration polarization term occurs when at the limiting current density; at this point the cell can't provide any additional current.

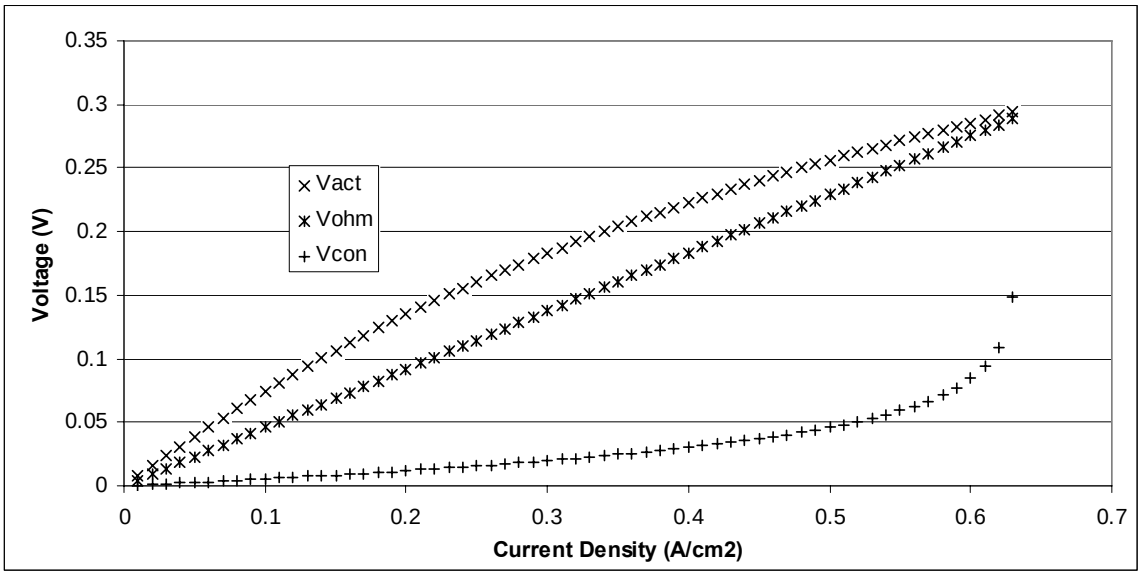

Figure 3.1 Cell polarization as a function of current density at a temperature of 1245 K and U_f of 0.75.

Figure 3.2 presents a comparison between the model and experimental data. These data were published by Singhal and Kendall (2004), but acquired from the Siemens Corporation. The U_f was 0.85, temperature was 1213 and 1272 K (2 separate runs) and the fuel was 89% hydrogen and 11% water. The temperature, U_f and mole fraction information were input to the model to produce the results presented in Figure 3.2. From Figure 3.2 it can be seen that the results fit the data reasonably well; the average relative error between the experimental data and the model data was 3.6 and 2.7% while the root mean square error was 3.1 and 1.9% for temperatures of 1273 and 1213 respectively. However, it appears that the model presents a stronger dependence with temperature then is evident from the Siemens data. Also, the data is not linear in the ohmic region of polarization. Other parameters such as operating pressure, experiment run time, and any associated errors or standard deviations were not available for the Siemens data. Without

that information it is difficult to properly evaluate the model with respect to the Siemens data. Nevertheless the model did produce results that overall fit well with the experimental data.

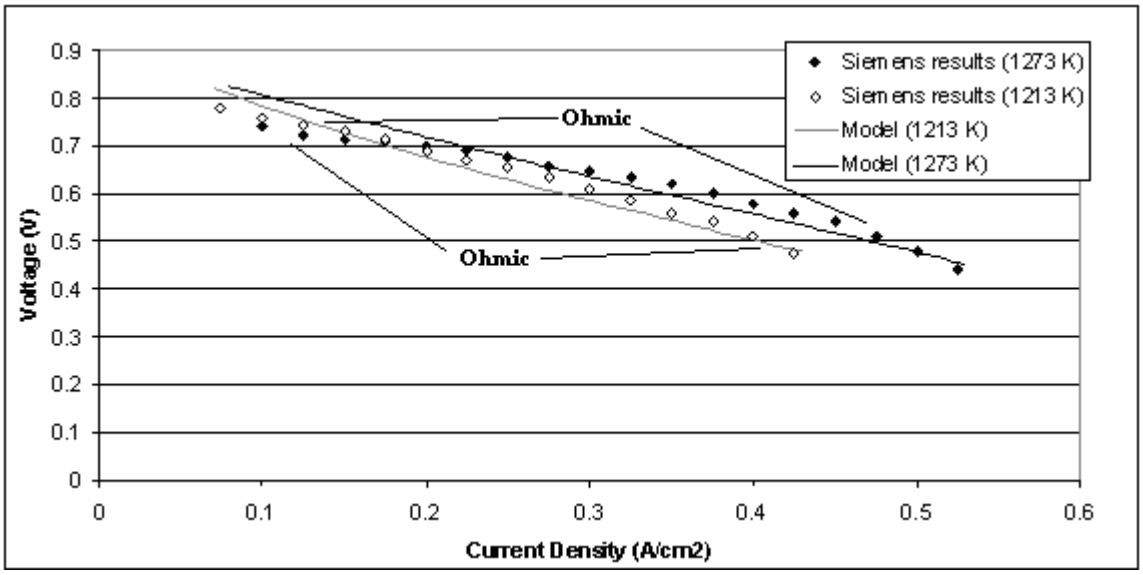

Figure 3.2 Comparison between model and experimental voltage vs. current density results from Kendall et al. (2004). The results are presented for two temperatures 1213 and 1273K with fuel utilization of 0.85 and a 0.11/0.89 water/methane fuel mixture.

3.2 Stack Results

Predictions using the Annex 42 model with the new cell level model, the stack resistance, and the energy balance were compared to experimental results collected by NRCan from a FCT fuel cell test system. Figure 3.3 presents the stack voltage versus stack current as calculated by the model as well as the experimental data. Data used to calibrate the Annex 42 model (BOP power draw and β_i ect.) with the new capabilities is termed "experimental" on Figure 3.3 and data used for blind comparison is termed "Validation". The experimental results are presented as averages of long run times in the order of hours. Similarly the results from the Annex 42 model with the new capabilities are generated

from long simulation times, in which the same P_{el} values from the experiments were used as inputs into the model. The U_f in the stack, the excess air ratio and the average stack temperature were also consistent between the series of model simulations and the experimental data they were being compared to. However, it should be noted that those parameters were not held constant in each separate experiment or simulation run. The average operating conditions for NRCan data are presented in Table 3.1.

Table 3.1 Calibration and validation operation parameters measured during each of the NRCan experimental runs using the FCT system. The parameters are averages of the values collected over the course of the experiments which ranged in length from 1-10 hrs.

	Pel(Watt)	Lambda	Fuel Utilization	Temperature(K)
Calibration Case 1	3010	2.59	0.756	1245
Calibration Case 2	3283	2.68	0.756	1255
Calibration Case 3	3353	2.64	0.733	1257
Calibration Case 4	3580	2.58	0.733	1262
Calibration Case 5	3728	2.67	0.730	1262
Calibration Case 6	3712	2.63	0.731	1263
Calibration Case 7	3728	2.60	0.731	1262
Validation Case 1	3600	2.54	0.729	1258
Validation Case 2	3746	2.68	0.730	1262
Validation Case 3	3743	2.64	0.732	1262
Validation Case 4	3715	2.55	0.730	1250

Figure 3.3 demonstrates good agreement between the model and experimental results; the slopes of the lines are 0.00045 and -0.00044 respectively with the model results having an R^2 value of 0.93. Also, the average relative and root mean square errors were less then 1% for the current and voltage. Both the model and experimental results show voltage degradation as a function of current density as can be expected. However, the slopes of the lines on Figure 3.3 do not precisely correlate. This could be due to the stack resistance. In the model this term is taken as a constant value rather then a function of current. In reality stack resistance would likely be dependent on current density. There are two phenomena which could serve to explain the stack resistance; non-uniform

temperature and current reversal. In the case of the model a uniform stack temperature is assumed. In practice temperature would vary in the stack creating cells or areas within a cell with lower and higher voltage. However, the average of the varying voltages within the cell would be lower then that predicted using just a uniform stack temperature because of the relationship between voltage and temperature (Section 3.4.2). This issue would be less severe as average stack temperature is increased. Average stack temperature increases with current density because the irreversibility (polarization) in the SOFC results in heat generation. The second possible cause of the stack resistance is the occurrence of current reversal stemming from the system design. The FCT SOFC system is comprised of 2 Siemens technologies Beta units. Each Beta unit consists of 24 cells with 8 in series and 3 in parallel. If any of the 3 sets of 8 cells in series are producing different voltages then it is possible for current backflow and an associated voltage loss. Modeling of this issue is challenging because temperature, species and flow information would have to be known throughout the entire stack in order to individually calculate each cells voltage and current production. As a result the stack resistance is left as a constant parameter.

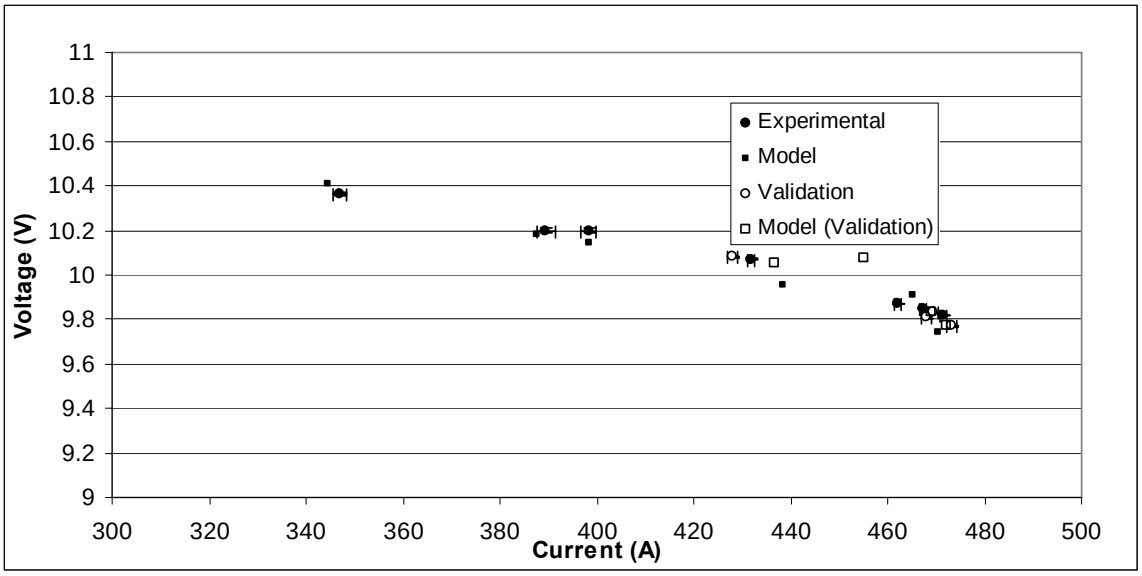

Figure 3.3 Comparison of model and NRCan experimental results for voltage vs. current performance of the SOFC stack.

Demonstration of the difference in performance between the cell and stack level is presented on Figure 3.4. On Figure 3.4 the Siemens cell data [Singhal and Kendall (2004)] is presented with the NRCan experimental data. There are a number of differences between the two experiments which should be identified before any conclusions are drawn. As previously reported the Siemens results used 0.85 U_f and an 89/11% split between hydrogen and water as fuel. The NRCan data was collected with a natural gas mixture, comprised of 95% methane [Beausoleil-Morrison, (2007)] as the fuel, 0.73-0.76 U_f and temperatures ranging from 1243-65 K. The higher U_f will limit the performance of the Siemens cell data (Section 3.4.1). However, the significantly larger partial pressure of hydrogen in the Siemens cell data will improve the performance of that system over the NRCan data (Equations 1.17-8, 2.25-6, 2.29). In order to compensate for the differences in operating parameters the model was run at the U_f, partial pressures and fuel composition of the Siemens and NRCan data. The difference between the two model results was then added to the NRCan data (Figure 3.4). Even with the corrected data, a

discrepancy exists between cell and stack data. As mentioned in Chapter 2 the stack resistance is used in the present research to account for the difference between cell and stack data.

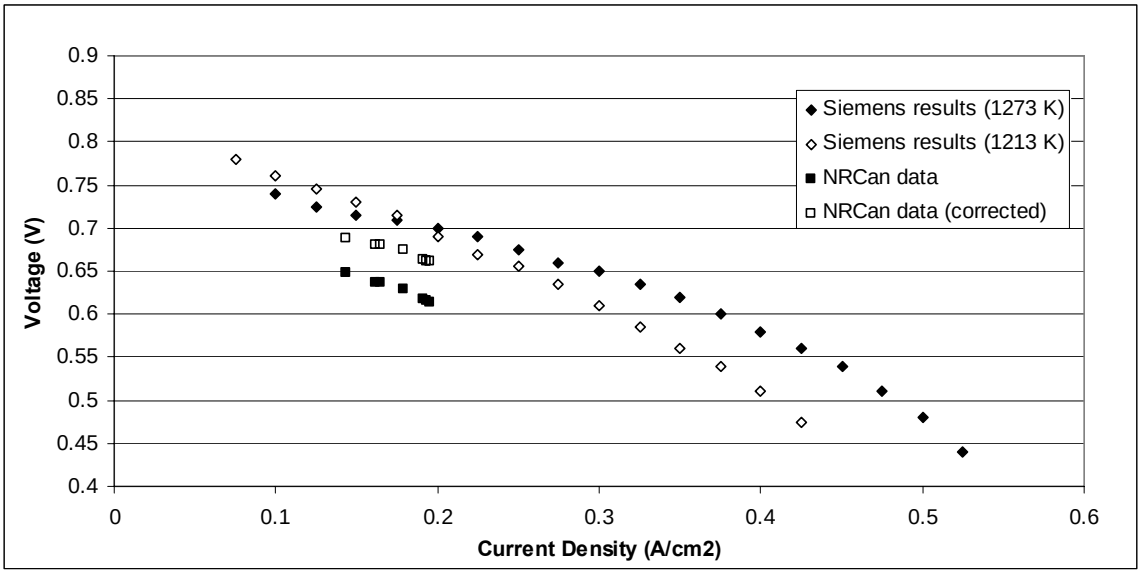

Figure 3.4 Comparison between Siemens and NRCan experimental data. Results are presented on a per cell bases, showing voltage vs. current density.

3.3 System Results

Figure 3.5 presents a comparison of the model results for η_{FCPM} (Equation 2.5) and the net electrical power (P_{el}). As on Figure 3.3 the data used only for validation and not for calibration is termed "Validation". The model and experimental results show good correlation; the average relative and root mean square error for η_{FCPM} were 1.3 and 0.53% respectively.

The figure demonstrates the role that the BOP components as well as the auxiliary burner fuel flow have on η_{FCPM}. Although with increasing power, η_{FCPM} initially drops until 3300 W, it begins to increase again after that. This might seem counter intuitive if one considers only that voltage losses increase with P_{el} and directly affect η_{FCPM} (Figure 3.3).

However, as P_{el} is increased the cell is able to maintain hotter temperatures and the burner is needed less frequently resulting in higher η_{FCPM} (see $\dot{N}_{fuel\text{-}burn}$ term in Equation 2.5). Furthermore, the higher temperatures result in higher reaction rate kinetics within the cell which also improves η_{FCPM}.

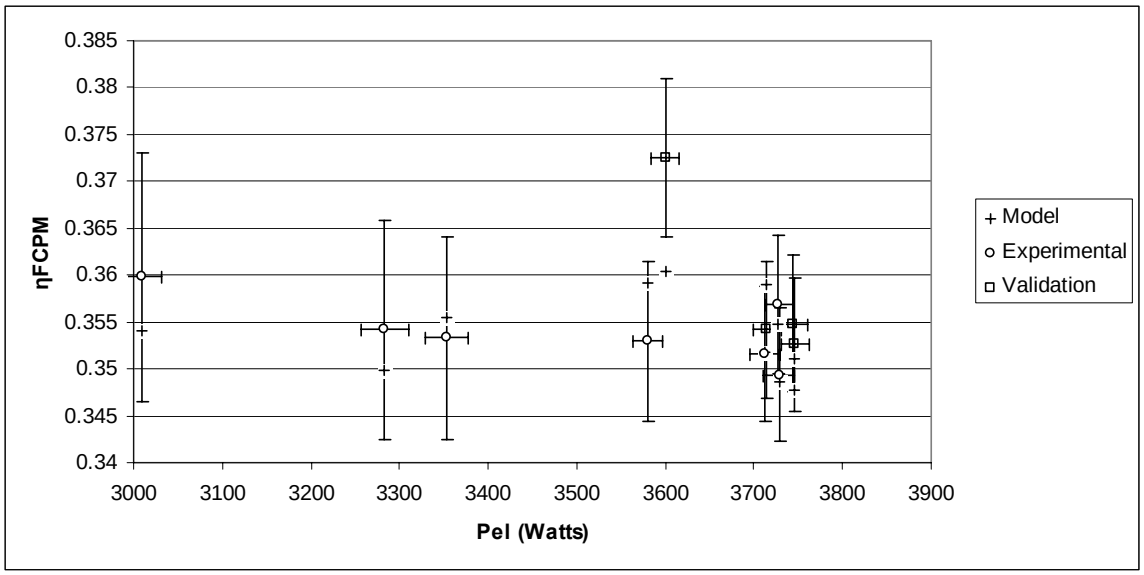

Figure 3.5 Comparison of model and NRCan experimental results for stack.η_{FCPM} as a function of $P_{el.}$

It should be mentioned that there is an additional cost with the new model in terms of simulation run time. The additional time is dependent on the desired precision of P_{el} and current results. For example in order to make sure that the model generates a voltage and current within 25W of the inputted P_{el} with a current prediction to the 0.001, would results in about 50% additional computational time for the electric plant network within ESP-r.

3.4 Demonstration of Improved Model Capability

One of the objectives of the current research was to generalize the Annex 42 model by incorporating a mechanistic model for the FCPM, and thus making the model less

dependent upon calibration parameters that must be derived from measurements on coherent systems. The improved model would be able to evaluate the effects of different operating parameters such as U_f, temperature and excess air ratio on the system and the fuel cell. The new modeling capabilities are demonstrated in the following sub-section by exploring the effects of the above-mentioned operational parameters. In the analysis the inputs from calibration data 1 (Table 3.1) were used unless otherwise specified.

3.4.1 Impact of Fuel Utilization on System Performance

Figures 3.6a and b present the results of the U_f analyses, the figure demonstrates the dependence of cell voltage on U_f; as U_f increase the voltage decreases. This result is logical considering the principles described in Chapter 2 (Equation 2.10). A lower U_f results in higher partial pressure or concentration of the reactants at the anode electrolyte interface available for the electrochemical reactions (Equations 1.15 and 2.9). The relationship is linear after a U_f of 0.67. In the analyses the average temperature of the FCV was 1245K (Calibration data 1, Table 3.1), however, at U_f below 0.67 the un-reacted fuel combusts and cause the temperature to rise (Figure 3.6b). The increased temperature improves the voltage performance of the fuel cell (Section 3.4.2).

From Figure 3.6a it can be seen that U_f does not have as large an effect on η_{FCPM} as it does on voltage. The effect is also not as straight forward. Between U_f of 0.64 to 0.72 η_{FCPM} increases, this may be counter intuitive as the stack voltage is decreasing. However, the reduced voltage results in more heat generation in the cell raising its temperature. The raised temperature means less fuel needs to be combusted in the stack

burner to maintain the set point temperature. Between U_f of 0.64 to 0.72 η_{FCPM} increases, this may be counter intuitive as the stack voltage is decreasing. However, the reduced voltage results in more heat generation in the cell raising its temperature. The raised temperature means less fuel needs to be combusted in the stack burner to maintain the set point temperature. At a U_f of 0.78 η_{FCPM} begins to decrease, this is because U_f is so high that there is not enough unreached fuel available for later combustion to maintain the operating temperature in the cell. As a result more fuel is required by the stack burner and η_{FCPM} would drop. Over all the effect of U_f on η_{FCPM} is not substantial in the range presented in Figure 3.6a. The nominal U_f of the FCT system was 0.73-0.76 during the NRCan experiments.

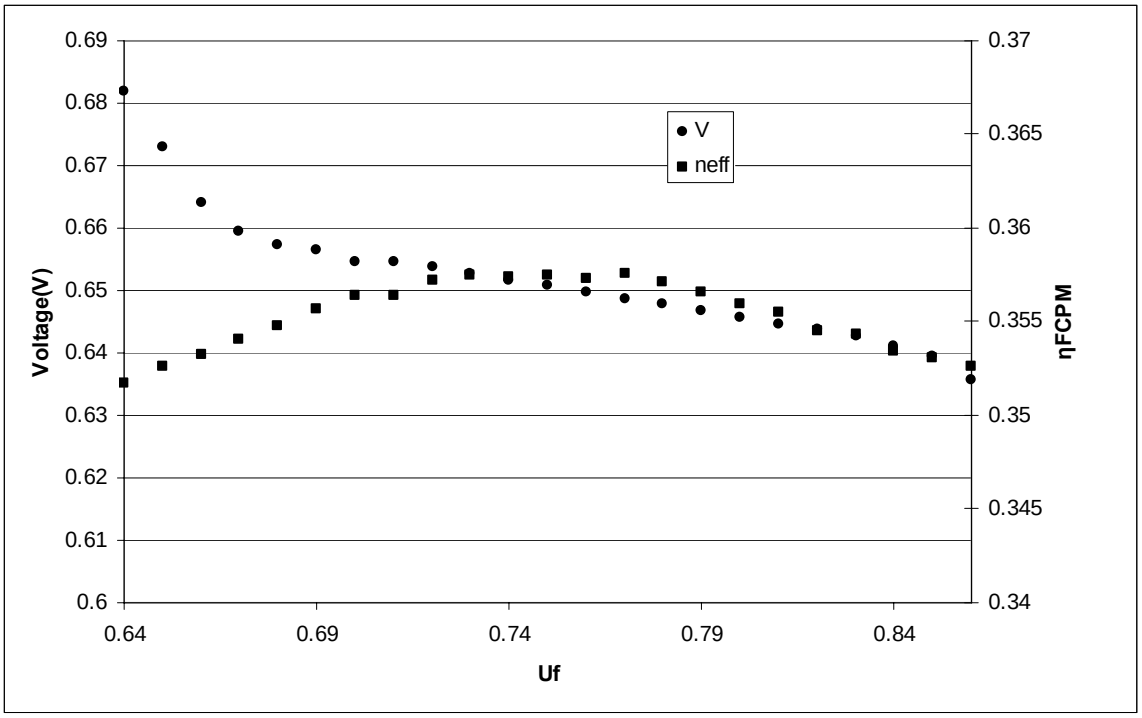

a)

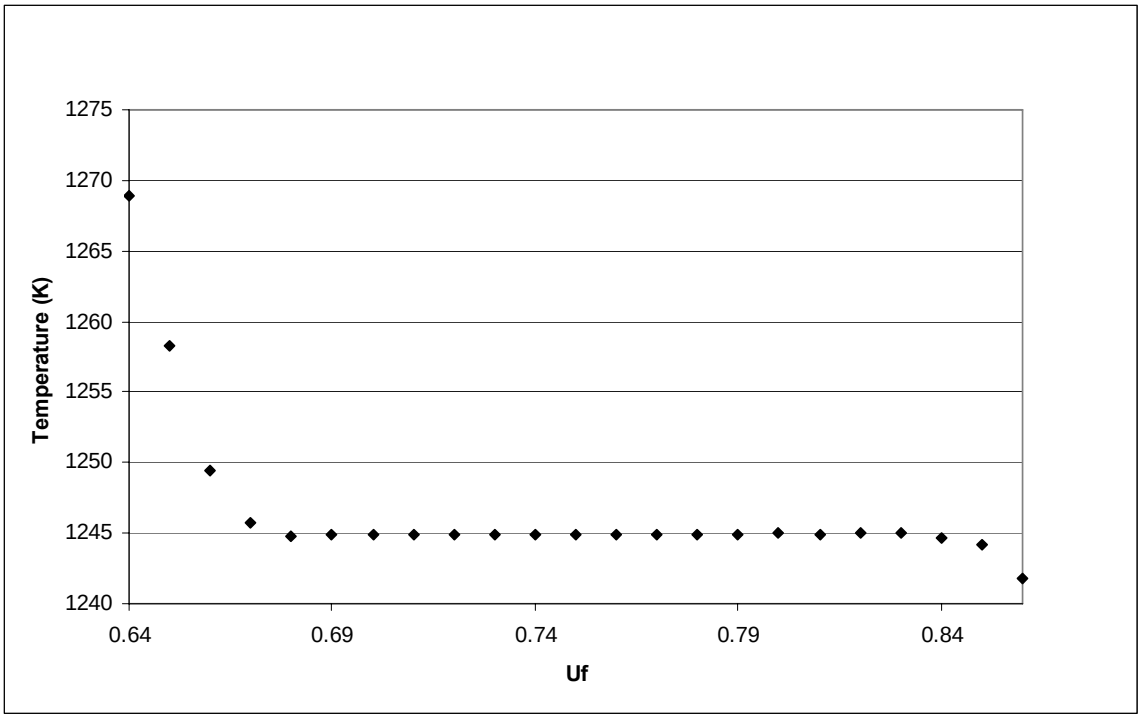

b)

Figure 3.6 Simulation results showing the effect of U_f on a) voltage and η_{FCPM} b) average stack temperature.

3.4.2 Set Point Temperature

Figure 3.7 presents the results from the temperature analyses and it's effects on system performance. During this analysis U_f was held constant at 0.76 and the average P_{el} was 3010 W. An upper and lower (burner off and on) were set for each simulation run 5 K apart, the average temperature is presented on Figure 3.7. Figure 3.7 demonstrates the strong correlation between temperature and voltage performance of the cell. The relationship is polynomial (quadratic) in nature with voltage increasing with temperature. The effect is expected due to the high temperature dependences of the polarization losses, especially ohmic (Equations 1.15, 1.17-8, 2.14-5, 2.18-19, 2.25-6, 2.29, 2.31-2).

Similarly to the U_f results, the effect of temperature on the entire system is not as straight forward as the effect on voltage. At temperatures bellow 1220 η_{FCPM} drops off because the voltage losses grow powerfully more severe. At temperatures above 1260 the amount of fuel required by the stack burner out ways the improved voltage performance associated with increasing temperature and η_{FCPM} drops off. Between temperatures of 1220-1260 K η_{FCPM} is steady. In that span the voltage is increasing as is the amount of fuel required by the stack burner. Based on the results (Figure 3.7) the effect of improved voltage performance (Equation 2.34) and increased stack burner fuel consumption (Equation 2.5) are balancing out causing η_{FCPM} to remain steady. In practice this region of steady η_{FCPM} is likely smaller. Although uniform stack temperature is assumed, non uniform temperature distribution in the stack could occur. If this occurs, cells or areas within a cell would experience lower then average temperatures. The "power" relationship between voltage and temperature would magnify those areas of reduced temperature resulting in decreased η_{FCPM} compared to those values reported by the model.

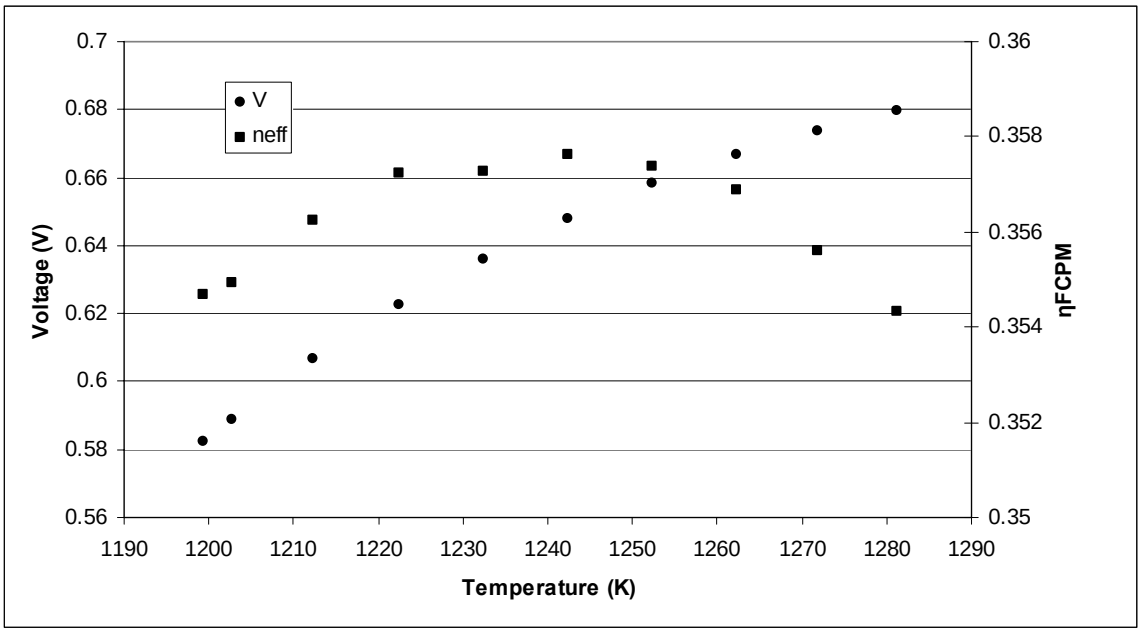

Figure 3.7 Simulation results showing the effect of average temperature on voltage and η_{FCPM}.

3.4.3 Excess Air ratio

Finally Figure 3.8 presents the effects of excess air ratio on η_{FCPM}. The effects are relatively straightforward. As excess air ratio is increased η_{FCPM} decreases. This result is logical from a thermodynamic stand point. The additional air added to the system must be heated, which requires more energy and reduces the η_{FCPM}. Logically then, reducing excess air ratio as much as possible (down to stoichiometry) would appear to be ideal. In practice, there are two reasons for not reducing excess air ratio right down to stoichiometry in an attempt to maximize η_{FCPM}. First, if excess air is reduced too much then insufficient oxygen will be available at the reaction sites and due to the mass transport limitations a substantial voltage loss could occur. Second, excess air ratio also provides additional cooling capacity to the system if temperatures rise.

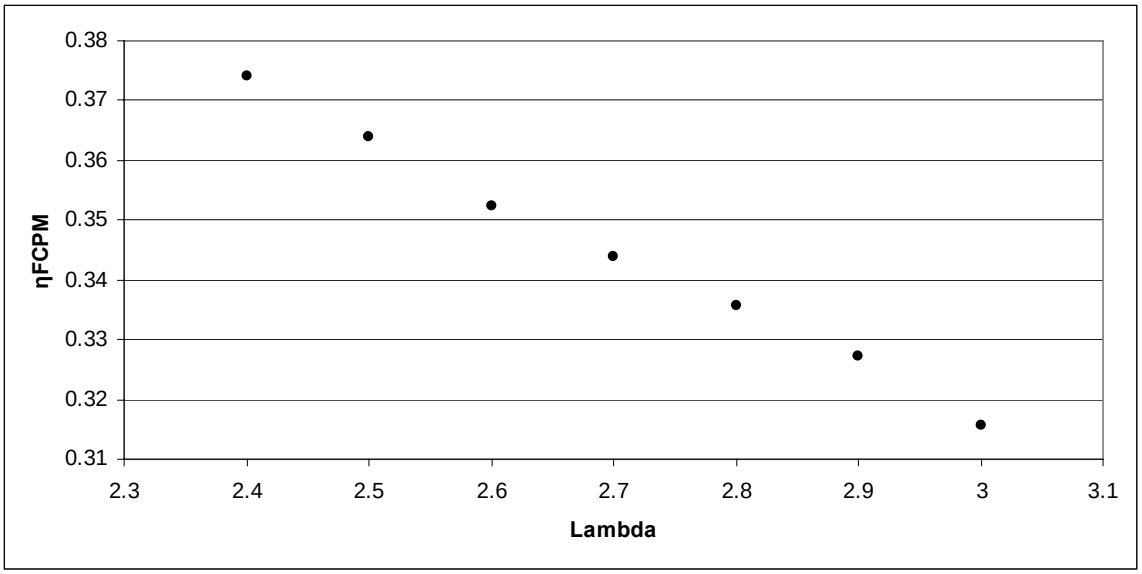

Figure 3.8 Simulation results showing the effect of excess air ratio on voltage and η_{FCPM}.

Chapter 4

Sensitivity Analysis

This chapter presents a sensitivity analysis aimed at demonstrating the robustness of the model and identifying the parameters to which the predictions are most sensitive. This in turn helps identify the degree of accuracy and reliability required in determining these parameters. The analyses performed are similar to those conducted on the operational parameters in chapter 3; however, operational parameters can be controlled by the system operator; whereas physical parameters are intrinsic to the system design. The physical variables being examined are characteristic of the SOFC materials as well as the fuel and oxidant participating in the reactions. Activation energy, material conductivity, diffusion rate, and the cell physical dimensions will be examined herein. During the sensitivity analysis all operational variables were held constant (Table 4.1).

Table 4.1 Operating parameters, used in sensitivity analysis.

Temperature (K)	1245
Uf	0.75
Lambda	2.59
Steam to carbon ratio	3.11
Fuel (100%)	methane

4.1 Activation Energy

Activation polarization accounts for a substantial voltage loss in SOFCs. As was discussed in Chapter's 1 and 2, activation polarization can be represented using the Butler-Volmer equation (Equation 1.16). The exchange current density in the Butler-Volmer equation is exponentially dependent on activation energy (Equations 1.17-8).

Therefore, percentage changes to activation energy have a large effect on the activation polarization, making activation energy a sensitive parameter. Figures 4.1 and 4.2 present the effect of altering the activation energy for both the anode and cathode exchange current densities. The changes to the activation energy are given in terms of % value used in the improved model.

Figures 4.1 and 4.2 demonstrate two important characteristics of the model. First that cathode side activation energy is much more influential on voltage loss then anode. Second that for both the anode and the cathode activation energies, the voltage loss and activation energy increase are not proportional, due to the exponential nature of the exchange current density (Equations 1.17-8). The significant voltages losses demonstrated in Figures 4.1 and 4.2 emphasize the importance of properly determining activation energies.

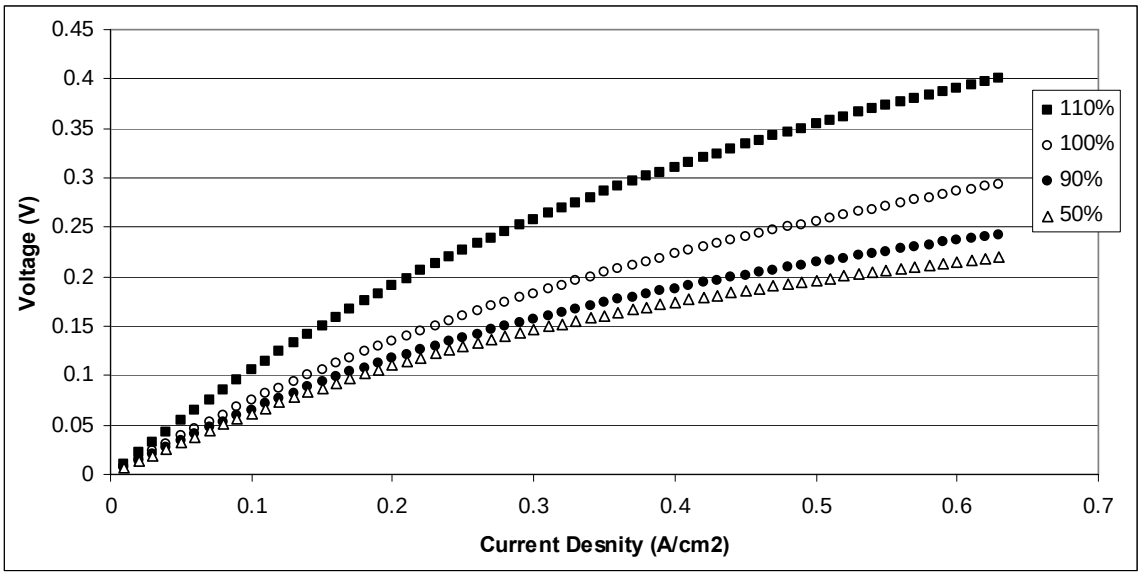

Figure 4.1 Voltage losses due to activation polarization for varying anode activation energy values.

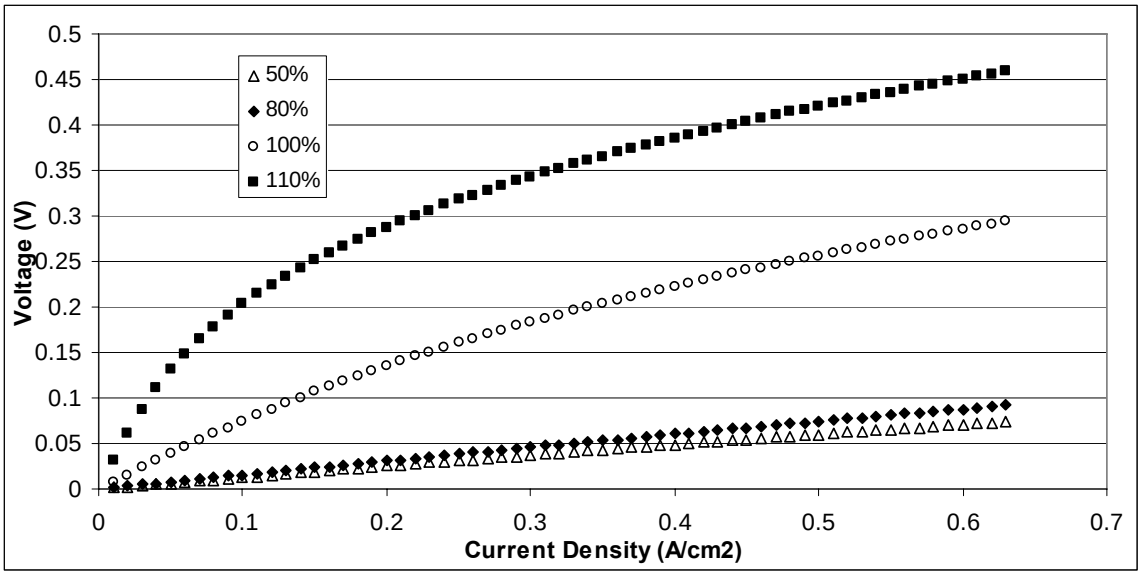

Figure 4.2 Voltage losses due to activation polarization for varying cathode activation energy values.

4.2 Conductivity

Ohmic resistance in SOFCs is due to the conductivity and arrangement of the electrolyte, electrodes and interconnect. Table 4.2 presents the results of altering the conductivities of each of the materials and thickness of each layer in the SOFC by 50 and 150%. From Table 4.2 it is obvious that reducing the conductivity of any of the materials will reduce the performance of the SOFC. Similarly, increasing any of those conductivities will improve it. The cathode and anode were the most sensitive to conductivity changes. This is because the current path of the anode and cathode is in the radial (θ-dir). This current path has a small area perpendicular to current flow causing increases in resistance (Equation 2.17a).

The effect thickness on the equivalent resistance of the cell is less straightforward than that of the conductivity. From Table 4.2 an improvement in equivalent resistance is seen

when the interconnect and electrolyte are 50% thinner. This raises the question as to why these layers are not reduced in thickness in the first place. The answer is that the layers are made as thin as possible without compromising other areas of the cell performance and its structural integrity. In the case of the interconnect reducing its thickness would put the cells closer together. Having the cells closer together could affect the amount of fuel available at the anodes of adjacent cells as the fuel flows through the increasingly thinning cell separation. Reducing the thickness of the electrolyte could result in electron or proton leakage from the anode to the cathode and reduce performance. Also thinning layers increase the manufacturing difficulty and expense. On the other hand the current path for the anode and cathode favours thickness, as can be seen in Table 4.2. Again the radial (θ-dir) current path has an increased perpendicular area (to current flow) as the cathode and anode gain thickness resulting in improved equivalent resistance. Increasing the thickness of the cathode and anode has the drawback of also expanding the diffusion path length resulting in reduced limiting current. This issue is discussed further in Sections 4.3 and 4.4

Table 4.2 Effect of conductivity and layer thickness on total equivalent ohmic resistance in a single SOFC cell.

Equvalent Resistance (ohm·cm^2)						
	Conductivity			Thickness		
	50%	100%	150%	50%	100%	150%
Interconnect	0.446	0.432	0.416	0.4155	0.432	0.448
Cathode	0.508	0.432	0.332	0.57	0.432	0.369
Electrolyte	0.459	0.432	0.398	0.398	0.432	0.459
Anode	0.505	0.432	0.330	0.563	0.432	0.368

4.3 Diffusion

Several parameters all have a proportional effect on limiting current density such as tortuosity, porosity and diffusion path (electrode thickness) (Equation 2.24). Therefore rather than adjusting each of those parameters individually, a sensitivity analysis was performed on the limiting current density itself. Figure 4.3 demonstrates that changes to cathodes limiting current density is minor compared to ohmic and activation polarization up to the point where the limiting current density is reached and diffusion dominates stopping current flow altogether. So, from Figure 4.3 it can be seen that improving the limiting current density can extend the maximum current a cell can provide, but provides very little benefit in terms of voltage. Only results for the cathode are presented in this report because altering the anode limiting current density by up to 200% was found to have little effect.

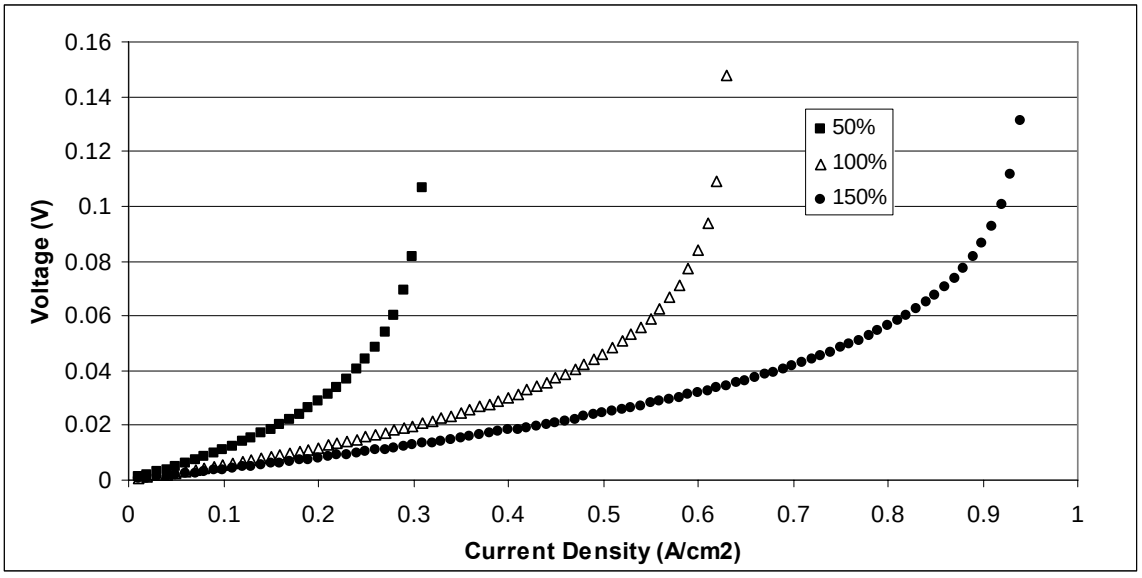

Figure 4.3 Voltage losses due to concentration polarization for varying cathode limiting current densities.

4.4 Cell Dimensions

The effect of anode, cathode and electrolyte thickness on the cell voltage is also examined. The results for the cathode are presented on Figure 4.4, the anode on 4.5 and the electrolyte on 4.6. As can be seen on Figure 4.4 neither reducing nor increasing the cathode thickness resulted in improved performance over the current FCT design. When the cathode thickness is decreased the ohmic resistance of the cell increases and the voltage drops. When the thickness is increased the ohmic resistance improves, but the concentration losses increase and the limiting current density for the cell is reduced. Therefore, based on the model results the present value for cathodic thickness are found to be a good compromise between limiting current density and equivalent resistance.

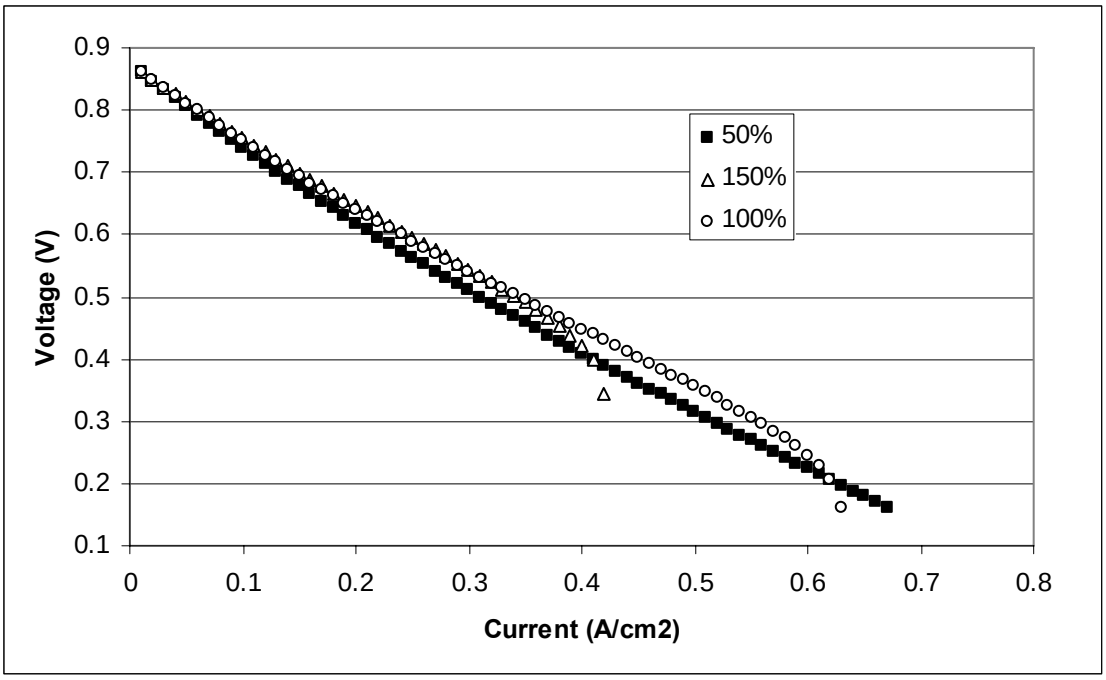

Figure 4.4 Cell voltage vs. current for % change to cathode thickness.

Increasing the anode thickness results in improved cell voltage even beyond the FCT cell design (Figure 4.3). The anode thickness and cathode thickness had similar effects on cell resistance, but the anode had much less of an influence on limiting current density as it was much thinner then the cathode (shorter diffusive path length). Therefore, improved ohmic resistance resulted in an increased cell voltage despite the degradation due to concentration polarization. Many current designs are moving towards planar designs having anode supported cells (anode layer supports weight and provides shape of cell), rather then cathode supported like the FCT stack. Perhaps results such as those presented on Figure 4.5 influenced this change.

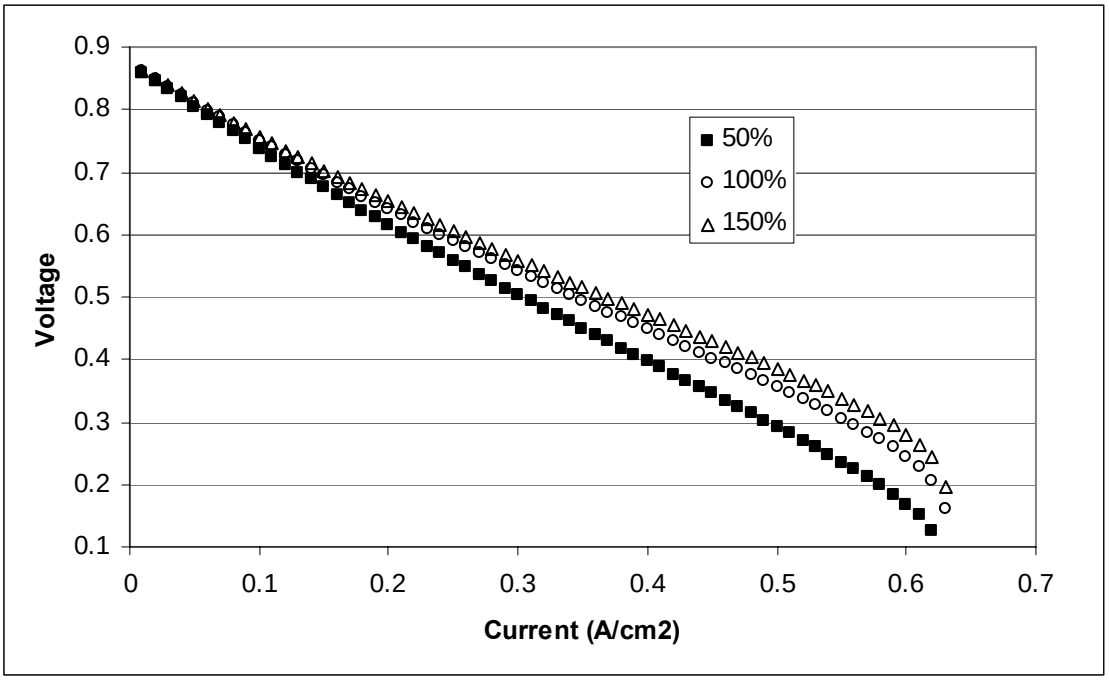

Figure 4.5 Cell voltage vs. current for % change to anode thickness.

Electrolyte thickness as discussed in Section 4.2 affects the ohmic losses of the cell through its effect on the equivalent resistance. Figure 4.6 demonstrates that reducing the thickness of the electrolyte improves equivalent resistance and consequently cell voltage.

As previously mentioned in Section 4.2, reducing electrolyte thickness can cause cell leakage and present potential manufacturing difficulties. Therefore, it is unlikely that tubular SOFC cell designer can significantly reduce the electrolyte layer thickness.

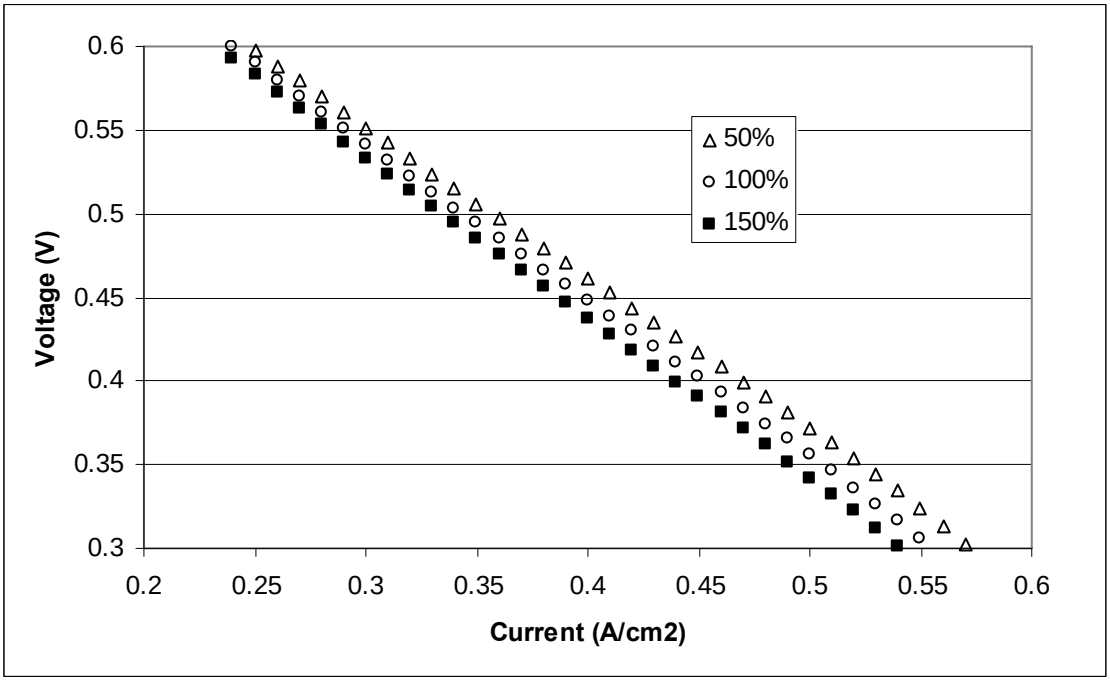

Figure 4.6 Cell voltage vs. current for % change to electrolyte thickness.

Chapter 5

Conclusion and Recommendations

5.1 Conclusions

This research set out to improve the treatment of the FCPM within the Annex 42 SOFC cogeneration system model that had previously been implemented into the building simulation program ESP-r. Previously a simple empirical equation was used to represent the electrical conversion efficiency of the entire FCPM. The objectives of the research were to:

1) Develop a semi-mechanistic model of the fuel cell stack.
2) Develop an appropriate energy balance of the fuel cell.
3) Calibrate and validate of the new FCPM model using existing experimental data.
4) Demonstrate the improved model's capabilities.

A semi-mechanistic fuel cell model was developed and coupled with an energy balance of the FCPM. The fuel cell model and energy balance were then implemented into the ESP-r building simulation program. Based on the results (Figures 3.3 and 3.5) the new model demonstrated good correlation with experimental data. Data produced by the model was within the uncertainty of the NRCan measurements with a R^2 value of 0.93 and slope of 0.45 compared to 0.44 for the NRCan data. Operating parameters such as U_f, set-point temperature, and excess air ratio, can all be altered in the improved model. Physical parameters such as activation energies, conductivity, diffusion parameters, and cell dimensions can also be altered for the purpose of evaluating other cell configurations,

newer designs, and hypothetical systems. These contributions substantially expand the capabilities of the Annex 42 model.

Several conclusions can be made regarding the operation of residential cogeneration SOFC systems based on the results of the current research:

1) A discrepancy exists between cell and stack voltage degradation

The general approach for stack and system level models found in the current literature consisted of a cell level model multiplied by the number of cells in the stack, coupled with an energy balance of the stack or system. The current research found that additional voltage losses occur at the stack level compared to the cell level. Literature reviewed for the current research did not determine this because model results were compared to single cell data rather then stack data. The stack resistance term was added to the model to account for these losses. Although the term was not large (3.55mV), it still demonstrated that consideration must be given when applying a cell model to a stack or system.

2) Sensitivity to temperature

Both the model and NRCan experimental results showed that between a P_{el} of 3000 and 3700 (W) the average stack temperature can rise from less then 1245 to greater then 1260K. These high temperatures and sensitivity to operational changes show that thermal management is important in SOFCs. The excess air ratio and the stack burner can be used to partially control temperature (Sections 3.4.2 and 3.4.3). However, the control is limited; if SOFC systems such as the FCT unit are to be implemented in residential cogeneration, temperature sensitivity must be carefully considered during installation and operation from both a performance and safety standpoint.

3) Improvements to voltage degradation must be met with improvements to thermal management or improved material properties at lower temperatures.

The current research demonstrated that improved cell voltage results in less heat generation (voltage losses or irreversibilities result in heat generation in SOFCs). If the reduced heat generation results in a temperature reduction sufficient to activate the stack burner then little or no gain in efficiency of the entire system will occur. Therefore, as improvements are made to the cell, better thermal management and material properties must also be researched to offset the reduced heat generation due to irreversibilities.

5.2 Recommendations

The new model compared well with experimental results while providing improved capabilities. Although the current research met all of its objectives, the following recommendations can be made for further research.

1) Implementation of a 1D cell and energy model

An average stack temperature was used in the cell model. The introduction of a 1D model would allow for a more accurate representation of temperature in the cell and in turn the voltage.

2) Improvements to characterization of BOP components

Equation 2.7 gives an example of a more theoretically based approach for determining the BOP power requirements. The current research did not implement this approach to generate any of the data presented in this report as the primary goal was to introduce and validate the improved fuel cell model as compared to NRCan's

FCT system data. Equation 2.7 could be further developed to apply to theoretical or other system configurations.

3) Better heat exchanger models

The current heat exchanger model (Equations 2.39 and 2.40) requires calibration with known system data for characterization of the heat exchanger effectiveness (β_i). In the same manner as the BOP components, heat transfer theory could be used to implement a heat exchanger model that does not relay on calibration.

These recommendations would provide a theoretical representation of the FCPM requiring no calibration. In order to implement this approach, all of the system materials, arrangement, and components would have to be known. For an entirely theoretically system this information could be researched or designed. However, for actual systems, such as the FCT device, it is doubtful that these recommendations could be performed as manufacturers may not reveal proprietary information on their systems.

References

Achenbach, E. “Three-dimensional and time-dependent simulation of a planar solid oxide fuel cell stack.” Journal of Power Sources, 49 (1994), 333–48.

Ahmed, K. Foger, K. “Kinetics of internal steam reforming of methane on Ni/YSZ-based anodes for solid oxide fuel cells.” Catal Today,63(2000), 479–87.

Akkaya, A.V. “Electrochemical model for performance analysis of a tubular SOFC.” International Journal of Energy Research, 31 (2007), 79-98.

Bavarsad, P.G. “Energy and exergy analysis of internal reforming solid oxide fuel cell–gas turbine hybrid system.” International Journal of Hydrogen Energy, 32 (2007), 4591-4599.

Beausoleil-Morrison, “Experiments for determined fuel.” IEA/ECBS’s Annex 42 Report (2007),

Bessette II, N.F. Wepfer, W.J. Winnick, J. “A Mathematical Model of Solid Oxide Fuel Cell.” Journal of the Electrochemical Society, 142 (1995), 11, 3792-3800.

Bessler, W.G. Gewies, S. Vogler, M. “A new framework for physically based modeling of solid oxide fuel cells.” Electrochimica Acta, 53 (2007) ,1782–1800

Bossel, U.G. Final Report on SOFC data facts and figures, Swiss Federal Office of Energy, Berne, CH, 1992.

Bove, R. Lunghi, P. and Sames, N.M. “SOFC mathematical model for systems simulation. Part one: from micro-detailed to macro-black-box model.” Hydrogen Energy, 30 (2005) 181-187.

Braun, R.J. Klein, S.A. Reindl, D.T. “Evaluation of system configurations for solid oxide fuel cell-based micro-combined heat and power generators in residential applications.” Journal of Power Sources, 158 (2006), 1290–1305.

Calise, F. D’ Dentice, M. Accadia, L. Vanoli, M.R. von Spakovsky “Single-level optimization of a hybrid SOFC–GT power plant.”, Journal of Power Sources, 159 (2006) 1162-1185.

Campanari, S. “Thermodynamic model and parametric analysis of a tubular SOFC module.” JPS, 92 (2001), 26-34.

Campanari, S. and Iora, P. “Definition and sensitivity analysis of a finite-volume SOFC model for a tubular cell geometry.” Journal of Power Sources. 132 (2004), 113-126

Chan, S.H. Khor, K.A. and Xia, Z.T. "A complete polarization model of a solid oxide fuel cell and its sensitivity to change of cell component thickness." JPS, 93 (2001), 130-140.

Chan, S.H. Ho, H.K. and Tian, Y. "Modeling of simple hybrid solid oxide fuel cell and gas turbine power plant." Journal of Power Sources, 109 (2002), 111-120.

Chan, S.H. Ho, H.K. and Tian, Y. "Multi level modeling of SOFC-gas turbine hybrid system" International Journal of Hydrogen Energy, 28 (2003), 889-900.

Chan, S.H. and Ding, O.L. (2005) "Simulation of a solid oxide fuel cell power system fed by methane." Journal of Hydrogen Energy, 20 167-169.

Damm, D., Fedrov, A. "Reduced-order transient thermal modeling for SOFC heating and cooling." JPS, 156 (2006), 956-967.

Dewitt, D.P. Incropera, F.P. Fundamentals of Heat and Mass Transfer. 5th Edition. Wiley, Toronto (2002).

Ferguson, J.R. Fiard, J.M., Herbin, R. "Three-dimensional numerical simulation for various geometries of solid oxide fuel cells." Journal of Power Sources, 58 (1996), 109-122.

Hawkes, A.D. Aguiar, P. Croxford, B. Leach, M.A. Adjiman, C.S. Brandon, N.P. "Solid oxide fuel cell micro combined heat and power system operating strategy: Options for provision of residential space and water heating." Journal of Power Sources, 164 (2007), 260-271.

Ivanov, P. "Thermodynamic modeling of the power plant based on the SOFC with internal steam reforming of methane." Electrochimica Acta, 52 (2007), 3921-3928.

Jia ,J. Abudula ,A. Wei, L. Jiang, R. Shen, S. "A mathematical model of a tubular solid oxide fuel cell with specified combustion zone." Journal of Power Sources .171 (2007.) 696–705.

Jiang, W. Fang, F. Khan, J.A. Dougal, R.A. "Parameter setting and analysis of a dynamic tubular SOFC model." Journal of Power Sources, 162 (2006), 316–326.

Kelly, N. and Beausoleil-Morrison, I. "Specifications for modeling Modelling Fuel Cell and Combustion-Based Residential Cogeneration Device within Whole-Building Simulation Programs.", IEA/ECBS's Annex 42 Report (2007), ISIBN 978-0-662-47116-5.

Kim, J.W. Virkar, A.V., Fung, K.Z. Mehta, K. Singhal, C. "Polarization Effects in Intermediate Temperature, Anode-Supported Solid Oxide Fuel Cells." Journal of the Electrochemical Society, 146 (1999), 69-78.

Krumdieck ,S. Page, S. Round, S. “Solid oxide fuel cell architecture and system design for secure power on an unstable grid.” Journal of Power Sources, 125 (2004), 189–198.

Larminie, J. Dicks, A. Fuel Cell Systems Explained. 1st Edition, Wiley, Toronto (2002).

Lisbona, P. Corradetti, A. Bove, R. Lunghi, P. “Analysis of a solid oxide fuel cell system for combined heat and power applications under non-nominal conditions.” Electrochimica Acta, 53 (2007), 1920–1930.

Lockett, M. Simmons, M.J.H. Kendall, K. “CFD to predict temperature profile for scale up of micro-tubular SOFC stacks.” Journal of Power Sources, 131 (2004), 243–246.

Massardo, A.F. Lubelli, F. “Internal Reforming Solid Oxide Fuel Cell-Gas Turbine Combined Cycles (IRSOFC-GT): Part A- Cell Model and Cycle Thermodynamic Analysis.” Journal of Engineering for Gas Turbines and Power, 122 (2000), 27-35.

Nagata, S. Momma, A. Kata, T. and Yasuhiro, K. “Numerical analysis of output of tubular SOFC with internal reformer.” JPS, 101 (2001), 60-71.

Nehter, P. “Two-dimensional transient model of a cascaded micro-tubular solid oxide fuel cell fed with methane.” Journal of Power Sources, 157 (2006), 325-334.

Nikooyeh, K. Jeje, A.A. Hill, J.M. “3D modeling of anode-supported planar SOFC with internal reforming of methane.” Journal of Power Sources, 171 (2007) 601–609.

Nisancioglu K. “Ohmic losses.” Proceedings of the IEA workshop on mathematical modelling, Charmey (1989), 87-98.

OPA. Ontario’s Integrated Power System Plan. Ontario Power Authority, Toronto., 2007

Padulles, J. Ault, G.W. and McDonald J.R. “An integrated SOFC plant dynamic model for power systems simulation.” Journal of Power Sources, 86(2000), 495–500.

Sanchez, D. Chacartegui1, Munoz, R. Sanchez , T. “On the effect of methane internal reforming modelling in solid oxide fuel cells.” International Journal of Hydrogen Energy, 33 (2008), 1834-1844.

Singhal, S.C., Kendall, K. High-temperature solid oxide fuel cells: fundamentals, design, and application, 1st Edition. Elsevier Advanced Technology, New York, 2003, 1.

Suwanwarangkul, R. Croiset, E. Pritzker, M.D. Fowler, M.W. Douglas, P.L. Entchev, E. “Mechanistic modeling of a cathode-supported tubular solid oxide fuel cell.” Journal of Power Sources, 154(2006), 74-85.

Suwanwarangkul, R. Croiset, E. Fowler, M.W. Douglas, P.L. Entchev, E. M.A. Douglas “Performance comparison of Fick’s, dust-gas and Stefan-Maxwell models to predict the

concentration over-potential of a SOFC anode." Journal of Power Sources, 122 (2003), 9-18.

Tanaka, K. Wen, C. and Yamada, K. "Design and evaluation of combined cycle system with solid oxide fuel cell and gas turbine." Fuel, 79 (2000), 1493-1507.

Virkar, A.V. Chen, J. Tanner, C.W. Kim, J.W. "The role of electrode microstructure on activation and concentration polarizations in solid oxide fuel cells." Solid State Ionics, 131 (2000), 189–198.

Westinghouse Report, High Temperature Solid Electrolyte Fuel Cell Power Generating Systems, D.O.E Annual Report (1981-82).

Wu,X.J. Zhu,X.J. Cao,G.Y. Tu, H.Y. "Nonlinear modeling of a SOFC stack based on ANFIS identification." Simulation Modelling Practice and Theory, 16 (2008), 399–409

Yoon, K.J. Zink, P. Gopalan, S. and Pal, U.B., "Polarization measurements on single-step co-fired solid oxide fuel cells (SOFCs)" Journal of Power Sources, 172 (2007), 39-49.

Zhang, W. Croiset, E. Douglas, P.L. M.D. Fowler, M.W. Entchev, E. "Simulation of a tubular solid oxide fuel cell stack using AspenPlusTM unit operation models." Energy Conversion and Management, 46 (2005), 181–196.

Zink, F. Lu, Y. and Shaefer, L. "A solid oxide fuel cell system for buildings." Energy Conversion and energy management, 48 (2007), 809-818.

Appendix A

Solution to Equation 1.10 (negative root not shown):

$$y=1/2/(1-U_F-K_S+K_SU_F)(3U_FCH_4^I-CO_2^I+K_SU_FCO^I-H_2O^IK_S+CO_2^IU_F-3CH_4^I-CO^IK_S-H_2^I-2KPSU_FCH_4^I+(2K_SCH_4^ICO^I+4K_SU_FCH_4^ICO^I+2CO_2^IH_2O^IK_S+12CO_2^IU_FCH_4^I+4K_SH_2O^ICO^I+10K_SH_2O^ICH_4^I+28K_SUF(CH_4^I)^2-2CO_2^IH_2^I-6CO_2^ICH_4^I+9(CH_4^I)^2-18U_F(CH_4^I)^2-4K_S(CH_4^I)^2-6U_F^2CH_4^IK_SCO^I-10U_FCH_4^IH_2O^IK_S+2K_S^2U_FCO^IH_2O^I+2K_SU_F^2CO^ICO_2^I+8K_S^2U_F^2CO^ICH_4^I-6UF^2CH_4^ICO_2^I-24U_F^2(CH_4^{I)2}K_S+K_S^2U_F^2CO^{I2}-2K_S^2U_F(CO_I)^2-2H_2O^IK_S^2CO^I+16K_S^2U_F^2(CH_4^I)^2-6U_FCH_4^IH_2^I+2CO_2^ICO^IK_S+2H_2O^IK_SH_2^I+2CO_2^IU_FH_2^I+2CO^IK_SH_2^I-16K_S^2U_F(CH_4^I)^2-4K_S^2H_2O^ICH_4^I+4K_S^2CH_4^ICO^I+4K_SCO_2^IH_2^I+12K_SCO_2^ICH_{4I}+9U_F^2(CH_4^I)^2+(CO_2^I)^2-2(CO_2^I)^2U_F+(H_2O^I)^2K_S^2-2H_2O^IK_SCO_2^IU_F+(CO_2^I)^2U_F^2+6CH_4^IH_2^I+(CO^I)^2K_S^2+(H_2^I)^2+4K_S^2(CH_4^I)^2+8H_2O^IK_S^2U_FCH_4^I+8CO_2^IU_F^2K_SCH_4^I-12CO^IK_S^2U_FCH_4^I-4CO_2^IK_SUFCO^I-20CO_2^IK_SU_FCH_4^I-2K_SU_FCO^IH_2^I+4H_2^IK_SU_FCH_4^I-4K_SU_FCO_2^IH_2^I-4U_FK_SH_2O^ICO^I)^{0.5})$$